Published online 21 February 2022

Nucleic Acids Research, 2022, Vol. 50, No. 11 ***e61***
https://doi.org/10.1093/nar/gkac113

ALT-FISH quantifies alternative lengthening of telomeres activity by imaging of single-stranded repeats

Lukas Frank[1], Anne Rademacher[1], Norbert Mücke[1], Stephan M. Tirier[1], Emma Koeleman[1], Caroline Knotz[1], Sabrina Schumacher[1], Sabine A. Stainczyk[2,3], Frank Westermann[2,3], Stefan Fröhling[4,5], Priya Chudasama[6] and Karsten Rippe[1,*]

[1]Division of Chromatin Networks, German Cancer Research Center (DKFZ) and Bioquant, Heidelberg, Germany, [2]Hopp Children's Cancer Center (KiTZ), Heidelberg, Germany, [3]Division of Neuroblastoma Genomics, German Cancer Research Center (DKFZ), Heidelberg, Germany, [4]Division of Translational Medical Oncology, National Center for Tumor Diseases (NCT) Heidelberg and German Cancer Research Center (DKFZ), Heidelberg, Germany, [5]German Cancer Consortium (DKTK), Heidelberg, Germany and [6]Precision Sarcoma Research Group, German Cancer Research Center (DKFZ) and National Center for Tumor Diseases (NCT), Heidelberg, Germany

Received July 28, 2021; Revised February 01, 2022; Editorial Decision February 01, 2022; Accepted February 05, 2022

ABSTRACT

Alternative lengthening of telomeres (ALT) occurs in ∼10% of cancer entities. However, little is known about the heterogeneity of ALT activity since robust ALT detection assays with high-throughput *in situ* readouts are lacking. Here, we introduce ALT-FISH, a method to quantitate ALT activity in single cells from the accumulation of single-stranded telomeric DNA and RNA. It involves a one-step fluorescent *in situ* hybridization approach followed by fluorescence microscopy imaging. Our method reliably identified ALT in cancer cell lines from different tumor entities and was validated in three established models of ALT induction and suppression. Furthermore, we successfully applied ALT-FISH to spatially resolve ALT activity in primary tissue sections from leiomyosarcoma and neuroblastoma tumors. Thus, our assay provides insights into the heterogeneity of ALT tumors and is suited for high-throughput applications, which will facilitate screening for ALT-specific drugs.

INTRODUCTION

Telomere maintenance mechanisms are crucial for the unlimited proliferation of cancer cells to counteract loss of chromosomal telomere repeats and senescence during the replication of linear chromosomes (1). The alternative lengthening of telomeres (ALT) pathway maintains telomere repeats at chromosomal ends in the absence of TERT, the protein unit of the reverse-transcriptase telomerase (2). ALT harnesses DNA repair and recombination activities (3,4) to synthesize telomeric DNA. Aberrant accumulation of telomere repeat-containing nucleic acids has been previously reported for ALT-positive (ALT+) cells of different origin. It comprises (i) accumulation of extrachromosomal telomeric DNA repeats (ECTRs) (5,6), (ii) the formation of both C- and G-rich single-stranded DNA at telomeric overhangs (7,8) or telomere-internal regions (9) and (iii) elevated levels of the telomeric repeat-containing RNA (TERRA) (10–12). Some of these telomere repeat-containing nucleic acids become enriched in specialized nuclear subcompartments (13,14) termed ALT-associated PML nuclear bodies (APBs) (15) and are also present in the cytoplasm (16,17). The C-circle (CC) assay detects ALT-specific C-rich telomeric DNA circles by rolling circle amplification and is currently the gold standard to quantitate bulk ALT activity of a cell population (18). Furthermore, we and others have applied immunofluorescence-based detection of APBs as an approach to detect ALT activity in single cells by fluorescence microscopy (15,19–21). However, the reliable APB quantification via co-localization analysis of telomere and PML signals is technically challenging (20,22). Moreover, the dynamic range of APBs as readout is limited since typical ALT cells only contain a few APBs per nucleus (20). In addition to cytological markers and CC analysis, sequencing-based strategies have recently provided insights into the aberrant ALT genome and transcriptome (12,23,24). However, the currently available sequencing readouts (e.g., ATRX/DAXX mutational status, telomere content, telomere variant repeat distribution, TERRA levels) do not provide single cell resolution and need to be cross-validated experimentally to reliably determine the ALT status (25). Thus, there is an unmet need for sensitive and more scalable ALT activity readouts to facili-

*To whom correspondence should be addressed. Tel: +49 6221 5451450; Email: karsten.rippe@dkfz.de

tate research, clinical diagnostics and drug screening. Furthermore, assays to characterize ALT heterogeneity at single cell resolution are crucial to identify rare cell phenotypes or ALT transition states contributing to tumor evolution. Here, we show that single-stranded DNA and RNAs containing the C- or G-rich telomere repeat sequences represent reliable markers of ALT activity that can be quantitated by a FISH-based ALT detection assay (ALT-FISH) *in situ*.

MATERIALS AND METHODS

C-circle (CC) assay

CC assays were performed based on the protocol described in (18) with some modifications. Genomic DNA (gDNA) was extracted from pellets of 2×10^6 cells using the Puregene core kit (Qiagen) and concentrations were determined using the Qubit dsDNA broad range kit (Thermo Fisher Scientific). The gDNA from leiomyosarcoma tumors was isolated as described in (24). CC reactions were set up in technical triplicates and including reactions without polymerase as negative controls. A total of 20 ng of gDNA was diluted in 10 μl nuclease-free water and mixed with 10 μl of the 2× amplification master mix containing 0.2 mg/ml BSA (New England Biolabs), 0.1% Tween-20, 2 mM DTT, 1 mM of each nucleotide and 7.5 U of phi29 DNA polymerase (New England Biolabs) in supplied enzyme buffer or a corresponding volume of water (negative controls). The reactions were incubated in a PCR cycler for 8 h at 30°C, then at 65°C for 20 min. The samples were diluted by adding 60 μl of 2× SSC buffer (0.3 M sodium chloride, 0.03 M sodium citrate, pH 7) and transferred onto a Roti-Nylon plus 0.45 μm membrane (Carl Roth) using a dot microfiltration apparatus (Bio-Rad, Cat. no. 170-6545). The membranes were dried for 10 min at room temperature, baked for 20 min at 120°C and washed in 2× SSC. CC amplification products were detected using the TeloTAGGG telomere length assay kit (Roche). In brief, membranes were prehybridized for 60 min at 42°C before incubation in 10 ml of the provided hybridization solution containing 30 nM digoxigenin-labeled telomere probe overnight at 42°C on a rotator. The next day, membranes were washed twice for 5 min with 2× SSC + 0.1% SDS at room temperature, twice for 15 min with 0.2× SSC + 0.1% SDS at 50°C and rinsed in 30 ml washing buffer for 5 min, followed by 30 min incubation with blocking solution. Anti-DIG-AP Fab fragments (Roche) were added to a final concentration of 75 μU/ml and membranes were incubated for 60 min, followed by two 15 min washing buffer incubations. Membranes were then rinsed for 2–5 min in detection buffer and incubated for 10 min with 1–2 ml CDP-Star chemiluminescent substrate solution (Roche) for detection on a Bio-Rad Chemi-Doc MP system. Intensities on membrane images were quantified using the Imagelab 6.0.1 software of the instrument. In brief, the integrated density value of each dot was determined from equally sized circular regions and subtracted from a local background value. The value of the no amplification control was subtracted from each sample and technical replicates were averaged to yield the raw CC level of a given sample on a given membrane. Unless stated otherwise, CC levels were always expressed relative to an U2OS reference sample (20 ng) from the same membrane to normalize for variations between membranes. An U2OS gDNA dilution series (4, 8, 16, 32, 64 ng of template per reaction) with corresponding no amplification controls was loaded onto each membrane to assess assay linearity within the specified working range.

Telomerase repeated amplification protocol (TRAP) assay

TRAP assays were performed as described in (26). A total of 1×10^5 of detached cells were pelleted by centrifugation for 5 min at 3000 g. The pellet was frozen and stored at −80°C for later use or used freshly by resuspending it in ice-cold NP-40 lysis buffer (10 mM Tris–HCl pH 8, 1 mM $MgCl_2$, 1 mM EDTA, 1% (v/v) NP-40, 0.25 mM sodium deoxycholate, 10% (v/v) glycerol, 150 mM NaCl, 5 mM 2-mercaptoethanol, 0.1 mM protease inhibitor) at a concentration of 500 cells/μl and incubation for 30 min on ice. For one reaction, a lysate equivalent of 500 cells pre-diluted in 5 μl nuclease-free water was added to 45 μl of TRAP master mix. After amplification, 20 μl of each reaction/lane was separated on a 12% TBE/polyacrylamide and visualized by SYBR Green staining.

Western blotting

About 10^6 cells were lysed in 100 μl ice-cold RIPA buffer containing Halt protease inhibitor cocktail (Thermo Fisher Scientific) for 1 h on ice. After removing insoluble components by centrifugation, the protein lysate concentration was determined using the BCA assay kit (Pierce). Per lane, 15 μg (30 μg in case of ATRX samples) of lysate was separated on precast 4–20% polyacrylamide gels (Bio-Rad) and transferred onto low-fluorescence PVDF membranes (Thermo Fisher Scientific) using the Trans-Blot Turbo transfer system (Bio-Rad). After blocking in 5% milk/TBS for 1 h at room temperature, primary antibody incubations were done in 5% BSA/TBST (0.1% Tween) overnight at 4°C. For improving signal quality, ATRX blots were incubated with a 1:1 mixture of two different rabbit anti-ATRX antibodies (see below). Membranes were washed three times in TBST before incubation with HRP- or fluorescently labeled secondary antibodies diluted in 5% milk/TBS or 1% BSA/TBST for 1 h at room temperature. After three TBST washes, the membranes were developed using the Clarity ECL western substrate (Bio-Rad) or, in case of fluorescently labeled antibodies, directly imaged on a Bio-Rad Chemi-Doc MP system. The following primary and secondary antibodies were used with the indicated dilutions: mouse anti-Tubulin (Calbiochem/Merck Millipore, CP06, 1:2000), rabbit anti-ASF1A (C6E10) (Cell Signaling Technology, #2990, 1:1000), rabbit anti-ASF1B (C70E2) (Cell Signaling Technology, #2902, 1:1000), goat anti-rabbit Alexa Fluor 568 (Life Technologies, A11036, 1:2000), goat anti-mouse IgG-HRP (Cell Signaling Technology, #7076, 1:2000), goat anti-rabbit IgG-HRP (Cell Signaling Technology, #7074, 1:2000), rabbit anti-ATRX #1 (Sigma-Aldrich, HPA001906, 1:500), rabbit anti-ATRX #2 (Cell Signaling Technology, #14820, 1:500).

Cell culture

All cell lines were maintained at 37°C in 5% CO_2 and split every 2–4 days using 0.05% trypsin/EDTA (Gibco) for detachment. MG-63, U2OS, Saos2, CAL72 and HeLa wt cell lines were cultured in DMEM medium containing 1 g l^{-1} glucose, supplemented with 10% doxycycline-free fetal bovine serum, 1× penicillin/streptomycin and 2 mM stable glutamine. HeLa ST, HeLa LT, MGBM1, SF188 cells were cultured in DMEM containing 4.5 g l^{-1} glucose and HOS cells in EMEM, both supplemented as described above. Human umbilical vein endothelial cells (HUVECs) (Lonza) were cultured in EGM-2 medium. NEM165, NEM157, NEM168 parental lines and ATRX knockout clones were maintained in Amniopan complete medium (PAN Biotech). U2OS, HeLa wt, CAL72 and Saos2 cells were obtained from the German Collection of Microorganisms and Cell Culture (DSMZ). HOS and MG-63 were purchased from CLS Cell Lines Services. NEM, MGBM1 and SF188 cell lines are described in (27) and HeLa ST and LT cell lines were kindly provided by Jan Karlseder (Salk Institute, USA) and are described in (28). All cell lines were tested for the absence of mycoplasma with the VenorGeM Advance kit (Minerva Biolabs) and were authenticated using single nucleotide polymorphism-profiling (Multiplexion).

Generation of transgenic and knock-out cell lines

The U2OS NCL-RFP cell line with red fluorescent nucleolin was generated with the pTagRFP-NCL vector from (29) by random stable integration of transiently transfected plasmid DNA and expansion of single resistant clones under antibiotic selection. HeLa H2A-YFP with yellow fluorescent histone H2A (30), the doxycycline-inducible U2OS-ATRX (31) and the NEM168 ATRX knock-out clones F2 and B5 (27) cell lines have been described previously. All transgenic cell lines were maintained and grown in media containing the appropriate selection antibiotics (0.75 mg/ml geneticin/G418).

ASF1 knock-down

HeLa cells were transfected with On-Targetplus Smartpool siRNAs (Dharmacon) targeting ASF1A (L-020222-02-0020, lot 200427) and ASF1B (L-020553-00-0020, lot 200427) or a non-targeting control pool (#D-001810-10-20) using the Lipofectamine RNAiMax transfection reagent (Thermo Fisher Scientific) according to the manufacturer's protocol. siRNA pools were reverse transfected at a final concentration of 1 nM of both the ASF1A and ASF1B pool or the control pool. For CC assay and western blotting, ∼1 × 10^6 trypsinized cells in 9.5 ml of culture medium were seeded into 10 cm culture dishes onto 500 μl transfection mix (9 μl RNAiMax reagent and 20 nM of each target pool or 20 nM of the control pool diluted in Opti-MEM (Gibco). The transfection was scaled down accordingly for the matching ALT-FISH samples (2.5 × 10^4 cells per well and 1 ml in 24-well plate with 12 mm coverslips). Cells were grown for 72 h after transfection before being processed for DNA isolation, protein extraction or ALT-FISH.

ATRX re-expression in U2OS

The doxycycline-inducible U2OS-ATRX cell line was used as described previously (31). To obtain matching CC assay and ALT-FISH data, 1 × 10^6 and 1.5 × 10^4 cells/ml/well were seeded into a T75 culture flask and a 24-well plate (containing 12 mm glass coverslips), respectively. The next day, ATRX expression was induced by exchanging the medium for medium containing 1 μg/ml doxycyline (Sigma-Aldrich). For each independent induction experiment, a corresponding T75 flask and 24-well plate were seeded and treated equally, but without the addition doxycycline (−dox control). The cells were grown for 72 h before being assayed. Cells growing in the flasks were trypsinized, washed once in PBS, snap-frozen as pellets of 1–2 × 10^6 cells (liquid nitrogen) and stored at –80°C until used for CC assay and western blotting. Cells growing in the matching 24-well plates were subjected to ALT-FISH as described below.

ALT-FISH on adherent cell lines

One day before the ALT-FISH staining, 5–8 × 10^4 cells/1 ml/well were seeded onto uncoated, sterile 12 mm round glass coverslips placed in standard 24-well cell culture plates. In the case of U2OS NCL-RFP/HeLa H2A-YFP co-cultures, 2.5 × 10^4 of each cell line were seeded per well. The grown cells were washed twice with PBS and then fixed for 20 min at room temperature by adding cold (–20°C) 70% ethanol. The fixed cells were washed twice with ALT-FISH washing buffer (100 mM Tris–HCl pH 8, 150 mM NaCl, 0.05% Tween-20) and excess buffer was carefully removed by tapping the coverslips on wipes. For an optional RNase treatment step, the coverslips were incubated at 37°C for 30 min in PBS containing 50 μg/ml RNase A (Thermo Fisher Scientific, EN0531) and/or 10 U/ml RNase H (New England Biolabs, M0297L) and then washed once again in washing buffer. Coverslips were then placed cell side down onto 30 μl of hybridization solution (2× SSC buffer, 8% de-ionized formamide, 5 nM fluorescent DNA probe) dispensed on parafilm and incubated in a humidified chamber for 20 min at 37°C. The two probes used were 5′-Atto 633-$(CCCTAA)_5$-3′-biotin (TelC) and 5′-Atto 633-$(TTAGGG)_5$-3′-biotin (TelG) manufactured by Eurofins Genomics (Germany). The biotin tag allows for additional binding for further downstream applications but was not used in the present study. After hybridization, the samples were rinsed twice in 2× SSC and incubated in PBS containing 5 μM DAPI (Sigma-Aldrich) for 15 min at room temperature in 24-well plates. For additional cytoplasm staining, coverslips were incubated in PBS containing 5 μM DAPI and 20 μg/ml TRITC-Phalloidin (Sigma-Aldrich) for 30 min at room temperature. Afterwards, the samples were washed three times (5 min each) with PBS, rinsed first with distilled water, then with 70% ethanol and finally dehydrated in 100% ethanol for 2 min. The samples were placed onto a clean paper wipe to dry for 5–10 min and mounted on standard 25 × 75 mm microscopy slides using Prolong diamond antifade mountant (Invitrogen).

Combined ALT-FISH and immuno-staining on adherent cells

ALT-FISH in combination with immuno-staining for PML, RPA, TRF2 and SUMO2/3 was carried out as described above until the 2× SSC washing steps after hybridization. Subsequently, the samples were washed twice in washing buffer and then fixed in 4% paraformaldehyde/PBS for 10 min at room temperature. After washing three times with PBS, the cells were permeabilized for 12 min in 0.2% Triton X-100/PBS at room temperature and washed again three times for 5 min in PBS. The samples were blocked in PBS containing 10% goat serum (blocking buffer) for 1 h and then incubated for at least 1 h on 30 μl primary antibody solution in blocking buffer dispensed on parafilm. After three 0.002% NP-40/PBS 5 min washes, the coverslips were incubated with blocking buffer containing fluorescently labeled secondary antibodies for 1 h. Following three washing steps in PBS (5 min), the samples were DAPI-stained, dehydrated and mounted as described for the standard ALT-FISH protocol above. The following primary and secondary antibodies were used with the indicated dilutions for immuno-staining of cell lines: mouse anti-PML (Santa Cruz, sc-966, 1:100), mouse anti-RPA (Abcam, ab2175, 1:300), rabbit anti-TRF2 (Novus Biologicals, NB11057130, 1:250), rabbit anti-SUMO2/3 (Abcam, ab3742, 1:200), goat anti-rabbit Alexa Fluor 568 (Life Technologies, A11036, 1:300), goat anti-mouse Alexa Fluor 488 (Life Technologies, A11029, 1:300).

Fluorescence correlation spectroscopy (FCS) for copy number estimation

FCS experiments were carried out on an LSM710 microscope equipped with a ConfoCor3 extension and a 40× water objective (NA = 1.2). A 633 nm laser was used for excitation together with a BP655-710nm emission filter. Measurements were conducted in 8-well chambered cover glass slides (Nunc LabTek). Alexa 633 dye (A33084, Molecular Probes) and Atto 633 labeled TelC ALT-FISH probe were diluted to a final concentration of 20 nM in 10 mM Tris–HCl pH 8, 10 mM NaCl, 0.002% Tween-20. Tetraspeck fluorescent bead 0.1 μm standards (Thermo Fisher Scientific, T7279) were used undiluted as provided by the manufacturer at ∼300 pM concentration. FCS data were fitted with the ZEN 2008 software using a single component fit.

ALT-FISH on cells in suspension

Cells in suspension, adherently growing U2OS and HeLa cell lines were cultured to 70–90% confluency and detached using trypsin/EDTA. For ALT-FISH, 3×10^6 cells (1.5×10^6 of each cell line for U2OS/HeLa mixtures) were pelleted by centrifugation at 500 ×g for 5 min and resuspended in 150 μl of cold FACS buffer (1% v/v fetal bovine serum in PBS). The cells were fixed by adding them in a drop-wise fashion to a tube containing 1.5 ml of ice-cold 80% ethanol while vortexing, followed by incubation in a thermo-shaker (600 rpm) for 20 min at room temperature. After fixation, the cells were washed twice (1× in cold FACS buffer, 1× in ALT-FISH washing buffer) by pelleting as described above and resuspending in 1 ml of buffer. The pellet was resuspended in 900 μl hybridization mix (2× SSC, 8% formamide, 2 nM TelC-633 ALT-FISH probe) and incubated for 20 min at 37°C while shaking at 600 rpm. The hybridization mix was removed by centrifugation, followed by resuspension of the pellet in 1 ml of 2× SSC. The suspension was transferred to 1.5 ml low protein binding tube that had been pre-equilibrated for 5 min with FACS buffer. 2× SSC was removed by centrifugation and the final cell pellet was resuspended in 200 μl PBS and filtered through a cell strainer into 5 ml FACS tubes. Samples were stored at 4°C until imaged by microscopy.

Tumor samples

Leiomyosarcoma (LMS) tumor specimens and one matching normal tissue sample were collected from nine adult patients who had been diagnosed with LMS according to World Health Organization criteria at NCT Heidelberg and Heidelberg University Hospital, Heidelberg. The five ALT-positive samples (LMS28, LMS21, LMS23, LMS43, LMS26) and four ALT-negative samples (LMS25, ULMS07, ULMS06, LMS47) studied here have been characterized previously (24). Tumor histology and cellularity were assessed at the Institute of Pathology, Heidelberg University Hospital, prior to further processing. Patient samples were obtained under protocol S-206/2011 approved by the ethics committee of Heidelberg University and following written informed consent. Fresh frozen tissue sections (5–6 μm thickness) were generated and immobilized on SuperFrost Plus microscopy slides (Thermo Fisher Scientific) at the DKFZ/NCT Sample Processing Laboratory. For neuroblastoma (NB) tumor samples three ALT-positive (NBD11, NBD12, NBD130) and four ALT-negative samples (NBD1, NBD103, NBD114, NBD144) were analyzed by ALT-FISH and have been characterized previously (12). For ALT-FISH staining, fresh-frozen NB specimens (∼30–50 mm^3 volume) stored at –80°C were embedded in tissue freezing medium (Leica Biosystems), sectioned (5–6 μm thickness) using an Epredia CryoStar NX50 cryostat and immobilized on SuperFrost Plus microscopy slides (Thermo Fisher Scientific). Immobilized sections were stored at -80°C until further processing. The assignment of sample names and IDs for the LMS and NB tissue samples is given in Supplementary Table S1.

ALT-FISH staining on tissue sections

The samples were thawed for a few seconds at 37°C on a pre-warmed PCR cycler (slide holder) and then immediately fixed in 100% ice-cold methanol for 30 min at –20°C. The slides were incubated for 1 min in isopropanol and subsequently dried for 5 min at room temperature. The section-containing area on the glass slide was confined using a hydrophobic pen (Vector Laboratories) and 300–500 μl of 5 μM DAPI in PBS were added (no cover glass) for 15 min in a humidified chamber, followed by a one-minute PBS wash. Before staining, tissue integrity was confirmed by wide-field microscopy after mounting the samples in 70 μl PBS using a 24 × 50 mm cover glass. The cover glass was removed by briefly immersing the slides upside down in PBS. Subsequently, the slides were incubated for 2 min in ALT-FISH

washing buffer (100 mM Tris–HCl pH 8, 150 mM NaCl, 0.05% Tween-20). The washing solution was removed and 300–500 μl of hybridization mix (2× SSC, 8% formamide, 5 nM TelC-633 ALT-FISH probe) were added onto the confined area. The slides were incubated for 20 min at 37°C without cover glass in a humidified chamber placed inside a hybridization oven (ACD Bio). After hybridization, the slides were immersed two times for 1 min in 2× SSC at room temperature. All LMS and NB samples without pseudo hematoxylin/eosin (H&E) staining were subsequently fixed in 4% PFA/PBS for 10 min at room temperature, washed in PBS twice (1 min each) and mounted in 45 μl Prolong gold antifade mountant (Invitrogen) using a 24 × 50 mm cover glass. This additional fixation step preserves tissue integrity by preventing further changes, which can occur during storage and or imaging of the sections after mounting. The DAPI staining was performed after hybridization as described above for the LMS sample subjected to ALT-FISH and pseudo H&E staining by fluorescence microscopy (32). It was followed by five washes in PBS and one in distilled water (brief dipping). The sample was then stained with 300–500 μl of eosin staining solution for 1 min, which contained 1 volume eosin Y solution (Sigma-Aldrich) plus 9 volumes sterile-filtered Tris-acetic acid buffer (0.45 M, pH 6), briefly dipped 15 times in distilled water, followed by incubation for 15 min and then again for 2 min in 2× SSC (slide staining jar). For imaging, the sample was mounted as described above. Samples were imaged in liquid mounting medium immediately after the staining or kept at 4°C in a humidified chamber until imaging.

Combined ALT-FISH and immuno-staining on tissue sections

ALT-FISH on NB tissue in combination with immunostaining for NCAM was carried out as described above until the 2× SSC washing steps after hybridization. Subsequently, the samples were fixed for 30 min in 4% PFA/PBS, washed 1 min in PBS and permeabilized for 10 min in 0.2% Triton-X100/PBS at room temperature. Following permeabilization, the samples were processed exactly as described for the adherent cell line protocol described above. A volume of 300 μl dispensed onto the confined sample area was used for the blocking and antibody incubation steps. A primary mouse monoclonal antibody against human NCAM/CD56 (Thermo Fisher Scientific, MA1-06801) was used at a dilution of 1:200 in blocking buffer and stained with a 1:300 diluted Alexa Fluor 488-conjugated goat anti-mouse secondary antibody.

Confocal microscopy of cell line samples

Mounted ALT-FISH samples on coverslips were imaged on an Andor Dragonfly 505 spinning disc confocal system equipped with a Nikon Ti2-E inverted microscope and a 100x CFI SR HP Plan Apochromat Lambda S silicone immersion objective. Multi-color images were acquired using laser lines at 405 nm (DAPI), 488 nm (H2A-YFP, Alexa 488), 561 nm (NCL-RFP, Alexa 568, TRITC) and 637 nm (Atto 633) for excitation with a quad-band dichroic unit (405, 488, 561, 640 nm) and corresponding emission filters of 450/50, 525/50, 600/50 and 698/77 nm (or 685/47). Unless stated otherwise, all samples were recorded with the same laser intensity (15%), exposure time (250 ms) and gain (100) settings in both the 405 nm (DAPI) and 637 nm (Atto 633 ALT-FISH probes) channels. Settings were varied for the other channels but kept constant when comparison of absolute intensities between experimental sets was necessary. Images were recorded at 16-bit depth and with 1024 × 1024 pixels dimensions (pixel size: 0.1205 μm) using an iXon Ultra 888 EM-CCD camera. Coverslips were imaged by automated tile-scans (1% overlap between adjacent images) conducted at one or more selected positions (scan area: ∼0.1–2 mm^2). Occasionally, positions were recorded manually or in multiple smaller tile-scans for samples exhibiting a low cell density. Every tile was recorded as z-stack of 10 μm thickness with a z-step size of 0.2 μm (51 z-frames). U2OS NCL-RFP and HeLa H2B-YFP cell mixtures stained by ALT-FISH in suspension were imaged in PBS in 8-well chambered cover glass slides (Nunc Lab Tek) with the same settings.

Image processing, segmentation and quality filtering of cell line data

Multi-channel z-stacks were recorded as Imaris format 16-bit images (Fusion 2 software, Andor Dragonfly 505) and converted into TIFs using the FIJI Bio-Formats importer (33). Images were then imported into *R* Studio using the EBImage package (34). Segmentation of nuclei and spots, quantification of image features and fully-automated quality filtering (removal of segmentation artifacts, out-of-focus positions) was carried out using custom image analysis pipelines written in *R* and mainly based on the EBImage package and is available at https://github.com/RippeLab/ALT-FISH together with a more detailed description. In brief, maximum intensity z-projections were used for thresholding-based segmentation of objects (nuclei, cytoplasmic areas and spots). Nuclei were segmented in the DAPI and cytoplasmic areas in the TRITC-phalloidin channel. Nuclei touching the image borders or nuclei with no matching cytoplasm mask and vice versa were discarded. For images of ALT-FISH-stained cells in suspension, nuclei were excluded that were only partially within the specified focus volume. Cells with cytoplasm masks touching >100 pixels of the image borders were removed. Adjacent cell masks were separated using a watershed algorithm. To exclude segmentation artifacts like doublets or nuclei with highly irregular shapes, nuclei shape features were computed. Shape parameters were used to derive a nucleus shape quality score (NSQS) as follows: $(r_{max} \times r_{SD} \times \text{perimeter})/(r_{min} \times \text{area})$, where r corresponds to the radius and max, min and SD to the maximum, minimum value and standard deviation thereof. Cells with an NSQS >3 (empirically determined value) were excluded from the analysis. Using the nuclear and cytoplasmic masks as regions, the mean, median and standard deviation of pixel intensities were determined in each channel. Intensity values were also calculated for a region corresponding to the nuclear mask minus all spot masks of the same nucleus (nucleoplasm mask). For calculating the coefficient of variation (CV), the standard deviation

of the nuclear ALT-FISH intensity was divided by the mean nuclear intensity for each nucleus. Spot segmentation was only carried out in regions corresponding to the segmented nucleus and/or cytoplasm masks. Spots were segmented in the ALT-FISH (Atto 633) or in the TRF2 (Alexa 568) channel (for ALT-FISH/TRF2/PML immunostained samples) using the custom *R* function *makeSpotMask()* with the scripts provided at https://github.com/RippeLab/ALT-FISH/functions. The intensity threshold above which a pixel was considered a spot was calculated for each nuclear mask area individually as 2.5 times (or 2 times for TRF2 spots) the median nuclear intensity (background estimate) in the ALT-FISH channel (or TRF2 channel). Cytoplasmic ALT-FISH spots were segmented using a 2 times median threshold. All spot count data displayed in Figures 1–7 and Supplementary Figure S1-S6 are summarized in Supplementary data set 1.

Spot co-localization analysis

The fold-enrichment of a signal (DAPI, PML, TRF2, RPA, SUMO2/3) in each segmented spot mask of a nucleus (ALT-FISH spots or TRF2 spots) over background was determined as the ratio of the mean intensity in the spot mask area and the mean intensity in the corresponding nucleoplasm mask area. Spots with signal enrichment ratios larger than 1.5 were categorized as co-localizing with that signal. This cutoff value corresponds to the 99th percentile of the distribution of all spot enrichment ratios for the DAPI signal. This co-localization approach assumes that the DAPI signal is not enriched in the segmented spot areas and thus represents a measure of the signal enrichment observed by chance.

Confocal microscopy and image analysis of tumor tissue

Tissue sections were imaged on the above-mentioned microscope system using a 100x CFI SR HP Plan Apochromat Lambda S silicone immersion objective. Tile-scans (10% overlap) were recorded from a selected central region of the tumor section (~1.3–2 mm^2). Every tile was recorded as a z-stack of 20 μm thickness with a z-step size of 0.4 μm. Tile-scans were stitched using Fusion Stitcher (Fusion v2.3) or in FIJI (33) (pseudo H&E images). All analyses were performed on maximum intensity z-projections generated in FIJI. For ALT-FISH signal quantification, nuclei were segmented on the DAPI channel image using Cellpose v0.72 (35) (Model = cyto; LMS cell diameter = 80; NB cell diameter = 55). ALT-FISH spots were detected on the ALT-FISH channel image using the RS-FISH plugin in FIJI (36) (Sigma = 1.75, Threshold = 0.0011; default RANSAC parameters, no background subtraction; spot intensity filtering cutoff = 1700 ± 100). Spots were assigned to nuclei using custom workflows using the FIJI (33), KNIME (37) and *R* software (https://www.R-project.org/) (Supplementary Figure S7). Spots located outside the segmented nuclear masks were not considered. In brief, the final spot positions called by RS-FISH were drawn as single pixels of value 255 onto an empty (pixel values 0) 8-bit image of the same dimensions and the integrated density in each nuclear mask area (output from Cellpose) was determined to derive the number of spots per nucleus. Downstream analysis was performed in *R* using custom code and the Seurat v3 software (38). Nuclei overlapping with staining artifacts, e.g., large ALT-FISH probe aggregates and/or (auto-) fluorescent signals occurring close to blood vessels and tissue borders were identified by high intensity/low contrast in the ALT-FISH channel and subsequent visual inspection for each individual tissue image. The corresponding data points were omitted using a semi-automated custom workflow written in *R* (using the EBImage package). The remaining nuclei were binned into four ALT activity groups based on their spot count (no ALT = 0; low ALT = 1-2; ALT = 3-20, super-ALT > 20). To generate color-coded ALT activity maps, the nuclear masks of the different ALT activity subpopulations were mapped back to images using custom workflows in FIJI or KNIME/Napari (https://napari.org) to select the corresponding nuclear masks by their xy-coordinates and draw/overlay them onto an empty 8-bit image using FIJI.

Plotting, image display and statistical analysis

Plotting of data and statistical tests were carried out in *R* (*ggplot2* package) or in GraphPad Prism 9. All microscopy images shown correspond to maximum intensity z-projections. Merged or single channel images were generated using FIJI. Overlaid outlines of nuclei or cytoplasm areas were outputs of the segmentation procedures described above. The ALT-FISH signal was scaled in the same way for all images displayed in this study (but differently for tissue and cell lines) and no non-linear image transformations were applied for display. Pseudo H&E representations of tissues were generated from fluorescent DAPI and eosin signals using an image transformation procedure similar to the one described in (32).

RESULTS

ALT-FISH visualizes single-stranded telomeric DNA/RNA repeats of ALT cells *in situ*

We developed a FISH protocol that uses the DNA probes TelC (C-rich probe targeting $(TTAGGG)_n$ repeats) and TelG (G-rich probe targeting $(CCCTAA)_n$ repeats) to detect all single-stranded (ss) telomeric repeat species characteristic of ALT (TERRA, ECTRs, overhangs, internal loops) (Figure 1A). The protocol was optimized to encompass a single isothermal hybridization reaction for fast fluorescence microscopy detection without denaturing double-stranded genomic DNA. Probe binding conditions were adjusted for high signal-to-noise ratio and reproducibility across different sample types with a minimal number of liquid handling step. The two DNA probes selected provide complementary information. The TelC probe targets both TERRA and G-rich telomeric ssDNA repeats, while the TelG probe maps C-rich single-stranded regions as for example present in C-circles. An RNase treatment step before hybridization enables distinction between TERRA and telomeric DNA signals. ALT-FISH conducted on the ALT+ osteosarcoma cell line U2OS yielded nuclear and cytoplasmic spots clearly visible by microscopy (Figure 1B),

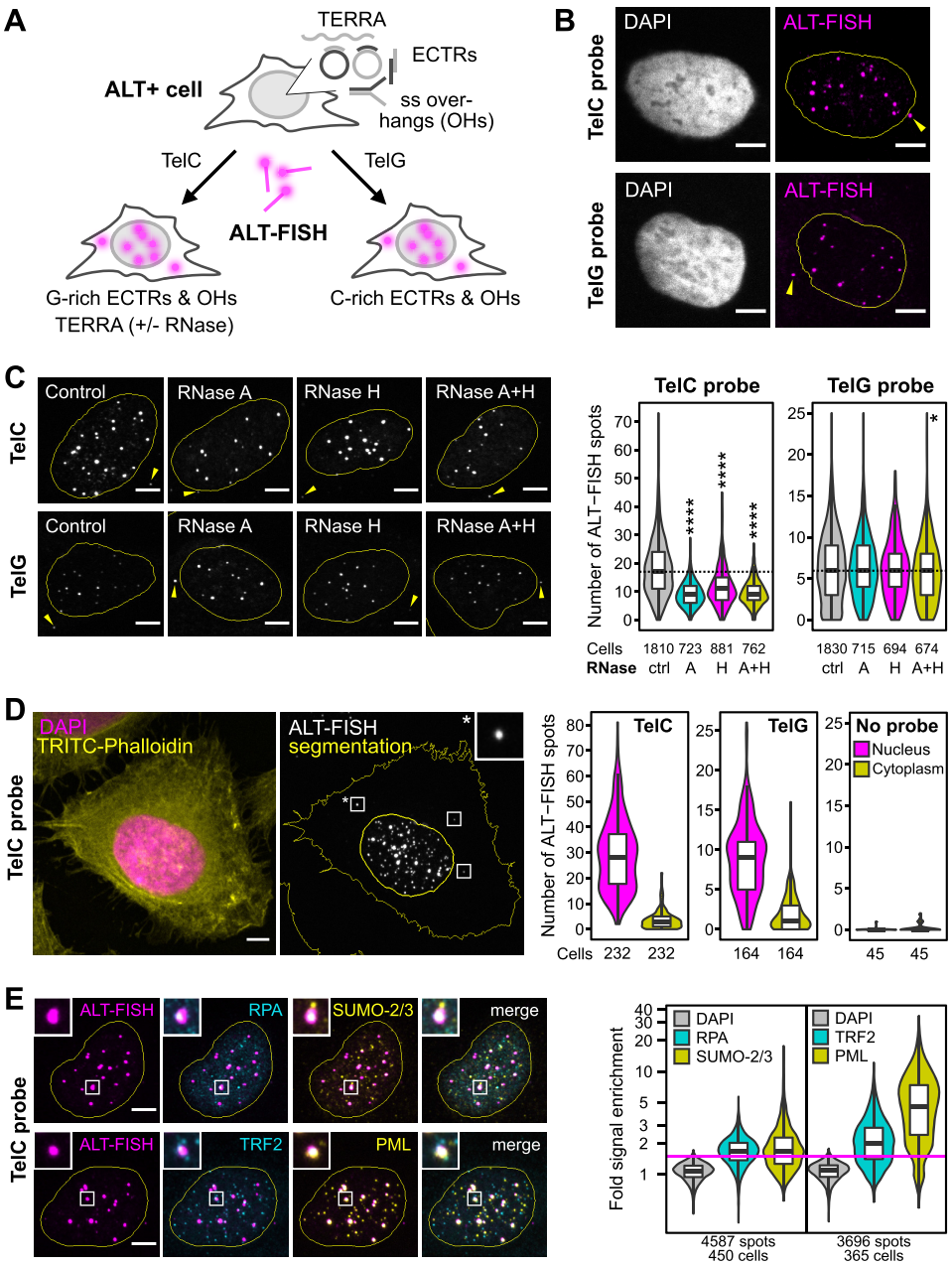

Figure 1. Detection and characterization of ALT-specific single-stranded telomeric repeats by ALT-FISH. (**A**) ALT-FISH detects ALT-specific single-stranded telomeric repeats that comprise TERRA, extrachromosomal telomeric repeats (ECTRs) and telomere overhangs by native FISH with probes targeting the G-rich (TelC) or C-rich (TelG) strand. RNase pre-treatment is used to quantify the contribution of TERRA. (**B**) ALT-positive U2OS osteosarcoma cells stained using Atto 633-labeled TelC or TelG ALT-FISH probes. Outlines show nucleus segmentation based on DAPI (arrows: cytoplasmic spots). (**C**) Comparison of ALT-FISH stained U2OS cells pre-treated with RNase A, H and RNase A + H or untreated (control, ctrl). Nuclear spots were quantified to assess the contribution of TERRA. Dotted lines mark the median spot number of the controls. Count data were pooled from 2–4 replicates. Adjusted *P*-values from a pair-wise Wilcoxon rank sum test with Benjamini-Hochberg (BH) correction compared to control groups were >0.05, 0.024 (*) or < 2e–16 (****). (**D**) Combined TelC ALT-FISH and DAPI/TRITC-phalloidin staining in U2OS cells to segment nucleus and cytoplasm (outlines) for spot counting with boxes/inset showing exemplary spots. The TelG probe and no probe control are depicted in Supplementary Figure S1F. Quantification for TelC, TelG or no ALT-FISH probe is shown as violin-boxplots. (**E**) Combined ALT-FISH and immuno-staining against APB marker proteins (PML, RPA, SUMO-2/3) and the telomere-binding protein TRF2 in U2OS cells (insets: typical co-localization events). See Supplementary Figure S1A for TelG probe. The plot for co-localization analysis shows the fold enrichment of each marker signal in the spot area relative to the nucleoplasm area for each segmented ALT-FISH spot. The DAPI reference signal was used to define a cutoff (>1.5, magenta line) above which enrichment was considered a meaningful co-localization. The cutoff-binned co-localization data are shown in Supplementary Figure S1B, D. All boxplots depict the median with first and third quartile of the distribution. The number of analyzed cells and/or spots is indicated below each plot. All scale bars are 5 μm.

indicating that the hybridizable DNA/RNA species organize into foci. The median nuclear spot number was 17 (TelC) and 6 (TelG), ranging from 0 to >60 spots and 0 to 25, respectively (Figure 1C). About half of the nuclear TelC but essentially none of the TelG spots were sensitive to RNase pre-treatment (Figure 1C). The spots displayed different intensities, indicative of different lengths of the single-stranded regions. We estimated the length of the hybridized ssDNA tracts to range from 0.3 to 41 kb (9-1388 FISH probes) per spot by comparing TelC spots in U2OS to fluorescent bead spike-ins of known brightness (Supplementary Figure S2I, J, Supplementary Table S2). Since ALT-FISH detects both chromosomal and extra-chromosomal repeats, we also quantified the number of cytoplasmic spots to specifically visualize single-stranded regions within ECTRs (Figure 1D, Supplementary Figure S1F). The cytoplasmic spots were less abundant and accounted for <10% of the total cellular signal in most cells (Figure 1D, Supplementary Figure S1G). These results corroborate previous studies examining cytoplasmic (16,39) or overall abundance (40) of ECTRs using denaturing FISH protocols. Immunofluorescence co-staining for the APB components RPA, SUMO2/3, PML and the telomere-binding protein TRF2 (Figure 1E, Supplementary Figure S1A) revealed that most ALT-FISH spots co-localized with these marker proteins. PML showed a particularly high enrichment (Figure 1E, Supplementary Figure S1A). The accumulation of the ssDNA-binding protein RPA further confirmed that ALT-FISH mainly detects ssDNA. Between 65 and 76% of TelC/TelG spots were enriched for both TRF2 and PML, while 23–26% co-localized with PML only (Supplementary Figure S1B, D). Segmentation of TRF2 spots and quantification of their PML and ALT-FISH signals showed that TRF2 spots with PML displayed higher ALT-FISH signal enrichment (Supplementary Figure S1C, E). Most TRF2 spots were devoid of PML and ALT-FISH signals (Supplementary Figure S1C, E), which is consistent with only a few telomeres being part of APBs. We conclude that ALT-FISH can visualize ALT-specific telomeric ssDNA/RNA species *in situ* to reveal their subcellular localization, length and interacting proteins. In agreement with previous studies describing APBs/PML bodies as reservoirs of ALT-specific nucleic acids (41), we found that telomeric repeats detected by ALT-FISH predominantly resided in APBs and in TRF2-free PML bodies.

ALT-FISH enables highly accurate separation of ALT+ and ALT- cells in cell mixtures

To test how well the ALT-FISH assay can distinguish ALT+ from ALT-negative (ALT-) cells within the same sample, we co-cultured the ALT+ U2OS NCL-RFP cell line (expressing nucleolin with red fluorescent protein) and the TERT+/ALT- HeLa H2A-YFP cell line (expressing histone H2A with yellow fluorescent protein) and stained them by ALT-FISH. TelC and TelG spots were clearly visible in U2OS cells but were mostly absent in HeLa cells (Figure 2A). We separated U2OS and HeLa cells based on their fluorescent marker signals (Figure 2B, E, Supplementary Figure S2B-E) and quantified the number of nuclear ALT-FISH spots. The median spot number was 0 for HeLa cells stained with either the TelC or TelG probe. In contrast, U2OS cells displayed a median number of 7.5 (TelG) and 12 (TelC) spots (Figure 2C, F). A cutoff of >2 ALT-FISH spots to separate ALT+ from ALT- cells was chosen to provide a high detection rate of 91–98% of ALT+ U2OS cells in the mixture with HeLa cells while maintaining a low false positive rate (FPR) of 0.8–3.4%. Calling of spots from images typically requires user-defined thresholding criteria, which makes the comparison of datasets analyzed using different segmentation algorithms difficult. We thus computed the nuclear coefficient of variation (CV) as an alternative measure of the ALT-FISH signal, which does not require spot segmentation. The CV method performed equally well for thresholds of >0.2 (TelC) and > 0.3 (TelG), retrieving 91–100% of ALT+ U2OS cells from the mixture with an FPR of 1.6–4.1% (Figure 2D, G). Next, the applicability of the ALT-FISH assay to cells in suspension was tested. We repeated the cell mixing experiment with trypsinized cells stained in solution using the TelC probe (Supplementary Figure S2A) and obtained comparable results (Supplementary Figure S2F–H). This confirms that the ALT-FISH hybridization reaction and the resulting signal are highly reproducible, making the assay suited for different types of samples and applications.

ALT-FISH predicts ALT status for various cancer cell lines

We next evaluated the specificity of ALT-FISH by assaying 6 ALT+ and 6 ALT-/ TERT+ cancer cell lines as well as primary HUVECs that have no active telomere maintenance mechanism (TMM) (Figure 3). The cell lines covered multiple cancer entities (osteosarcoma, pediatric glioblastoma (pedGBM) and cervix carcinoma) and their TMM was validated by both CC and telomerase activity assays (Supplementary Figure S3C, D). Two cell lines were classified as weakly ALT+ since they had no detectable telomerase activity and low CC levels. The median ALT-FISH spot numbers for ALT+ cell lines ranged between 7–17 (TelC) or 3–6 (TelG) (Figure 3A, B, Supplementary Figure S3A, B). In contrast, they were mostly between 0–1 for TERT+ and HUVEC or ranged between 0-2 for the weakly ALT+ cell lines. The MG-63 cell line represented an exception as it consistently displayed 1-2 spots for the TelG probe. Spot numbers were significantly higher when comparing all ALT+ cell lines to TERT+ or HUVEC, clearly separating them by ALT status ($P_{adj} < 2 \times 10^{-16}$, Wilcoxon rank sum test). In line with the co-culture experiment (Figure 2), a threshold of >2 nuclear spots was found to be optimal for classifying cells as ALT+ by ALT-FISH. Next, we evaluated the heterogeneity of ALT activity within the different cell lines. First, we found the signal distribution to be right-skewed (Figure 3B) with maximum ALT-FISH spot numbers as high as 11 times that of the population median. This extensive heterogeneity was common to all ALT+ cell lines. We defined the small population (5%) with a particularly high spot number at the long tail of the distribution as 'super-ALT' cells (Figure 3B). Second, we observed strikingly similar ALT-FISH profiles for the weakly ALT+ NEM165 and TERT+ (ALT-) HeLa LT (long telomeres) cell lines. Both displayed few cells (~4% and ~6%) with >2 TelC spots and had barely detectable CC levels

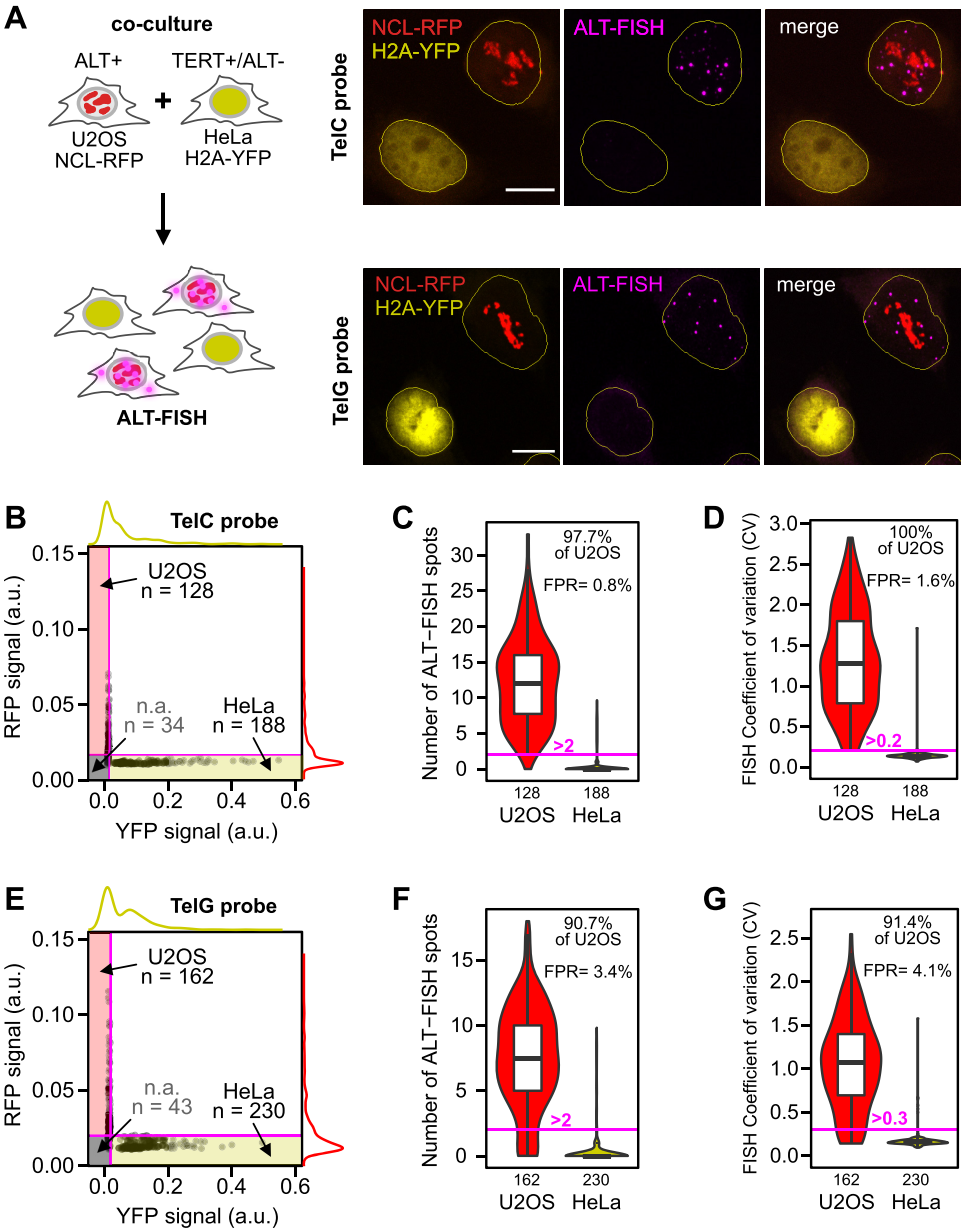

Figure 2. ALT-FISH distinguishes ALT+ and ALT- cells with high accuracy. (**A**) Co-culture of ALT+ U2OS NCL-RFP (red fluorescent protein) and TERT+/ALT- HeLa H2A-YFP (yellow fluorescent protein) to assess sensitivity and specificity of ALT-FISH with TelC or TelG probes. Outlines show nucleus segmentation from DAPI signal. Scale bars are 5 μm. (**B**) Scatter plot of RFP versus YFP mean nuclear intensity signal with marginal density diagrams for 350 cells from two independent co-culture experiments with TelC ALT-FISH staining. Cells were identified as HeLa or U2OS in the mixture using intensity thresholds (magenta lines, shaded areas) determined from the individual U2OS and HeLa cultures (Supplementary Figure S2B, C). Cells below these thresholds were excluded (not assigned, n.a.). (**C**) Distribution of nuclear TelC ALT-FISH spots in cells identified as U2OS or HeLa, respectively. The fraction of identified U2OS cells and the FPR are given for a separation cutoff of >2 spots. (**D**) Analysis of the same images as in panel C, but for the coefficient of variation (CV) of the nuclear ALT-FISH signal as an alternative parameter without spot segmentation (empirical cutoff > 0.2). (**E**) Same as in panel B but ALT-FISH staining with the TelG probe. A total of 435 cells from two independent co-culture experiments were analyzed. Intensity distributions of the individual cultures used for identity assignment are given in Supplementary Figure S2D, E. (**F**) Same as panel C but for the TelG probe. (**G**) Same as panel D but for the TelG probe. All boxplots depict the median with first and third quartile of the distribution.

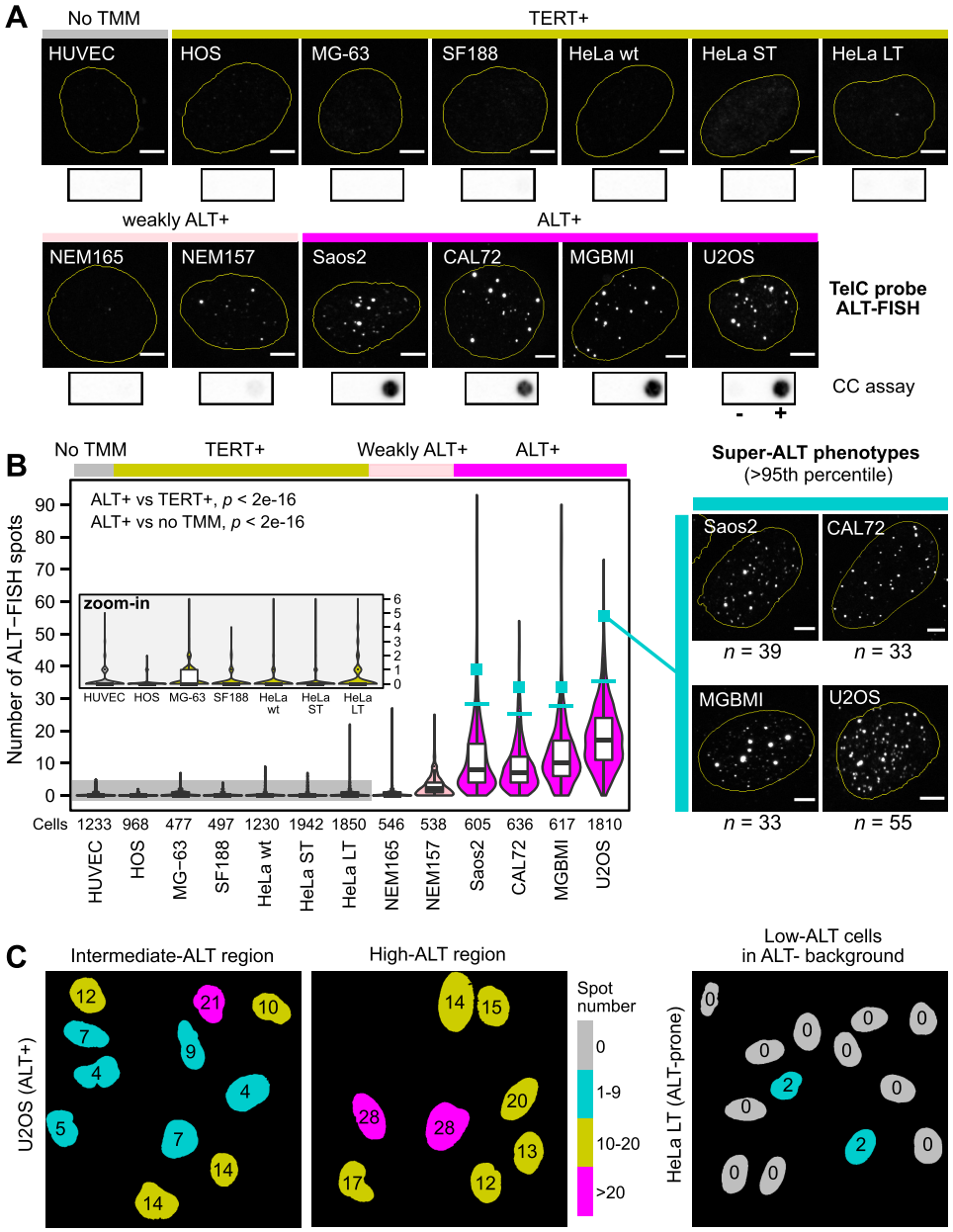

Figure 3. ALT-FISH predicts the ALT status of cell lines from different cancer entities and resolves cellular heterogeneity. (**A**) Representative images of a cancer cell line panel and primary HUVECs stained by TelC ALT-FISH. The telomere maintenance mechanism (TMM) is indicated above and representative CC assay results (+/– phi29 polymerase) are shown below (dot blot). Outlines represent nucleus segmentation. Corresponding results for the TelG probe are shown in Supplementary Figure S3A, B. CC and telomerase activity assays used to determine the TMM status are displayed in Supplementary Figure S3C, D. (**B**) Nuclear TelC ALT-FISH spot numbers for the cell lines shown in panel A. Count data were pooled from 2–4 independent replicates (cell numbers given below). U2OS data are the same as for the untreated control in Figure 1C. The spot distribution in the no TMM/TERT+ cell lines is magnified for better visualization. All boxplots depict the median with first and third quartile of the distribution. Adjusted *P*-values were calculated using a pair-wise Wilcoxon rank sum test with BH correction, comparing all ALT+ cell lines (including weakly ALT+) to the other groups (no TMM, TERT+). Cyan lines mark the 95th percentile of the spot number distribution in ALT+ cell lines above which cells were defined as super-ALT. Images of super-ALT phenotypes in Saos2, CAL72, MGBMI, U2OS with spot number *n* given below the image. The cyan box marks the position within the distribution shown on the left side. (**C**) Selected positions picked from U2OS (ALT+) and HeLa LT (TERT+, ALT-prone) TelC ALT-FISH to visualize ALT activity in a spatial context. Examples of intermediate and high-ALT clusters found in U2OS (left). Rare cells with low ALT activity found within the mostly ALT-negative HeLa LT population (right). Nuclear masks are color-coded by spot number (legend). All scale bars in images are 5 μm.

(<1% of U2OS levels, Supplementary Figure S3C). As opposed to HeLa cells with wild-type or short telomeres (ST), HeLa LT are telomerase-positive but can develop ALT when depleted of the histone chaperones ASF1A/B (28). These results suggest that the distribution of ALT-FISH signals at the population level can also inform about the propensity of a cell line to develop ALT. Cells with 1–2 spots were rare in ALT+ but more frequent in weakly ALT+ cell lines and HeLa LT, possibly representing states of low ALT activity. By integrating the spatial information from ALT-FISH images in U2OS and HeLa LT cells, we furthermore discovered that part of the heterogeneity seems to be spatially encoded. Cells with similar spot numbers were often found in close vicinity and there were regions with overall higher or lower ALT activity as well as confined hubs of low ALT activity in clearly ALT-negative regions (Figure 3C).

Following dynamics of ALT induction and suppression using ALT-FISH

Next, we determined how well ALT-FISH signals reveal changes in ALT activity. Three model systems were used for the perturbance of ALT activity: (i) TERT+ HeLa LT cells in which ALT was induced by siRNA-mediated knock-down of ASF1 (28), (ii) pedGBM NEM168 cells (27) that switch from a state of low to high ALT activity upon deletion of the ALT suppressor ATRX and (iii) inhibition of ALT activity in U2OS cells by inducing expression of the ALT suppressor ATRX (31). In the first approach, the depletion of ASF1A/B protein resulted in the expected CC level increase in HeLa LT cells that is indicative of ALT induction (Figure 4A–C). In agreement with these changes, both TelC and TelG ALT-FISH signals were increased for ASF1-depleted HeLa LT when compared to the controls (Figure 4D, Supplementary Figure S4A, B). TelG ALT-FISH signals correlated well with changes in CC level, suggesting that the TelG probe mostly detects CCs. We uncovered substantial heterogeneity in the response, as only a fraction of cells developed additional ALT-FISH spots. Strikingly, we also observed some TelC ALT-FISH signal changes in HeLa ST upon ASF1 depletion which remained undetected by the CC assay (Figure 4C, D). ALT induction has not been reported for HeLa ST previously and these observations show the power of ALT-FISH to visualize small ALT activity changes due to its single cell resolution.

The second cellular system for tracing changes in ALT activity involved the transition of the NEM168 cell line from a weakly to a strongly ALT+ state upon ATRX knock-out (Figure 4E, F). Similar to the ASF1 knock-down, we found that the number of nuclear TelC and TelG ALT-FISH spots correlated very well with increasing CC levels (Figure 4G, H). Moreover, the CC level difference of the two knock-out clones (B5, F2) (Figure 4G) was reflected in both the TelC and TelG spot number distributions.

To test if ALT-FISH captures a decrease in ALT activity, we used a previously established transgenic ALT+ U2OS cell line capable of expressing the ALT suppressor ATRX by addition of doxycycline (dox) (31) (Figure 5A). Three days of induction resulted in detectable ATRX protein expression in the otherwise ATRX-deficient cell line (Figure 5B). This was accompanied by ALT suppression as inferred from the strong reduction in CC levels to about 13% of wild-type levels (Figure 5C). It is noted that the uninduced U2OS-ATRX cell line also showed moderately reduced (69%) CC levels. However, this difference to the parental cell line was much smaller and is likely attributable to leakiness of the ectopic ATRX construct. ALT-FISH staining revealed the loss of TelG spots upon ATRX expression (median spot number; –dox: 6, +dox: 0) (Figure 5D). Thus, the TelG signal showed a very high correlation with CC abundance. In contrast, we found little agreement between the TelC spot number and CC level changes in this ATRX induction experiment (Figure 5C, D). Rather, the number of TelC spots was consistently higher for both the induced and uninduced U2OS-ATRX cells when compared to wild-type cells while spot features (intensity, area) remained similar (Supplementary Figure S5A, B). Since TelC ALT-FISH also detects TERRA, we assessed its contribution to the signal by RNase treatment before hybridization. TERRA is typically up-regulated in ALT but ALT activity is not the only regulator of TERRA expression (42–44). The RNase treatment before ALT-FISH revealed that TERRA levels were higher in the transgenic U2OS-ATRX model compared to wild-type cells and uncoupled from ALT activity as reflected by the CC levels (Supplementary Figure S5C). However, and in agreement with our TelG ALT-FISH results (Figure 5D), we found that the number of RNase-resistant TelC spots was well correlated with the changes in CC level (compare Supplementary Figure S5C and Figure 5C). We conclude that ALT-FISH reliably visualizes ALT activity changes in three independent models of ALT perturbation. Moreover, we find that the combination of TelC and TelG probe with RNase-treatment has advantages over TERRA-FISH, since TERRA expression can occur independent of ALT activity as apparent from the ATRX induction in U2OS cells.

ALT-FISH on primary leiomyosarcoma and neuroblastoma tissue sections maps tumor heterogeneity

Next, we applied ALT-FISH to patient tissue sections from nine leiomyosarcoma (LMS) tumors (five ALT-positive, four ALT-negative) and one matched normal tissue control (Figure 6) (24). To verify the robustness of ALT-FISH across different cancer entities, we furthermore expanded our analysis to seven neuroblastoma (NB) tumor samples (three ALT-positive, four ALT-negative) that were previously characterized in another study (12) (Figure 7). We established an automated image analysis workflow for fast and unbiased quantification of ALT-FISH spots in tissue images (Supplementary Figure S7, Materials and Methods). Quantification of ALT-FISH spots in ∼87 000 (LMS) to ∼106 000 (NB) individual cell nuclei across 20 analyzed tumor sections from two entities revealed generally lower spot counts in tissues as compared to cell lines (Supplementary Figure S6, Supplementary Data Set 1). However, tissue sections from ALT-positive tumors displayed ∼16-fold higher mean spot count per nucleus (1.21; 95% CI: 0.66–1.75) as compared to those from ALT-negative tumors and normal tissue (0.077; 95% CI: 0.016–0.14) when pooling LMS and NB samples. We used the available normal tissue control (LMS) (Figure 6) and normal tissue regions identified by IF staining in neuroblastoma (Figure 7) to de-

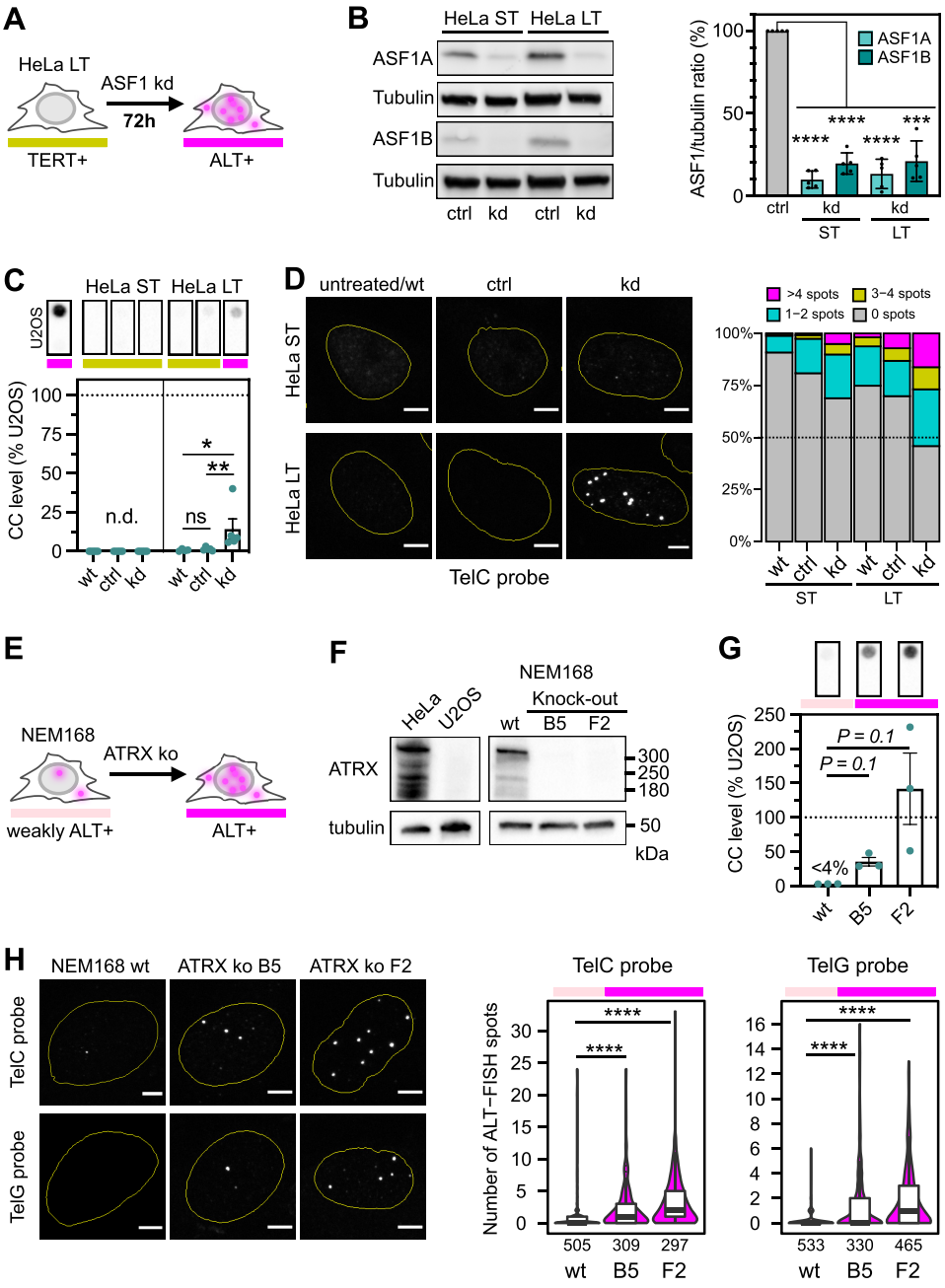

Figure 4. ALT-FISH visualizes ALT activity changes induced by ASF1 or ATRX depletion. (**A**) Scheme of ALT induction by ASF1 knock-down in the ALT-prone cell line HeLa LT (long telomeres). (**B**) Western blot and corresponding quantification to verify ASF1A/B depletion upon siRNA-mediated knock-down (kd) in HeLa LT and the control cell line HeLa ST (short telomeres). ASF1 levels were normalized to tubulin and a matched sample transfected with a non-targeting siRNA control (ctrl). Bar plots represent the mean and SD of 5 independent knock-down experiments with $P = 0.0001$ (***) and $P < 0.0001$ (****) from a one-sample Student's *t*-test. (**C**) Quantification of CC level changes upon ASF1 kd with representative blots on top. Bar plot depicts the mean and SEM of five replicates. All values are expressed relative to an ALT+ U2OS reference sample (n.d., not detectable) with $P > 0.05$ (not significant, n.s.), $P = 0.015$ (*) and $P = 0.0079$ (**) from a Wilcoxon rank sum test. (**D**) Exemplary TelC ALT-FISH stained cells and quantification for the ASF1 knock-down. Data from untreated/wt cell lines are included for comparison and are the same as in Figure 3B. Count data were binned for better visualization and are depicted as percentage fraction of all analyzed cells for each condition. For TelG ALT-FISH data and un-binned spot count data see Supplementary Figure S4. Data were pooled from three independent knock-down experiments. (**E**) Schematic of ALT activity induction by ATRX knock-out in weakly ALT+ pedGBM NEM168 cells. (**F**) ATRX western blot confirming loss of ATRX in the two NEM168 CRISPR knock-out clones B5 and F2 versus the parental cell line (wt). HeLa (ATRX wt) and U2OS (ATRX-deficient) are included as references. (**G**) CC level changes upon ATRX knock-out with representative blots shown on top. Bar plots depict the mean and SEM of three independent replicates. All values are expressed relative to an ALT+ U2OS reference sample. The *P*-values for the indicated comparisons were calculated using Wilcoxon rank sum test. (**H**) TelC and TelG ALT-FISH staining and nuclear spot number quantification for NEM168 wt and the two ATRX knock-out clones (B5, F2). Data were pooled from 2–4 independent replicates (cell numbers given below). Adjusted *P*-values from a pair-wise Wilcoxon rank sum test with BH correction were < 2e–16 (****). All boxplots depict the median with first and third quartile of the distribution. All scale bars are 5 μm.

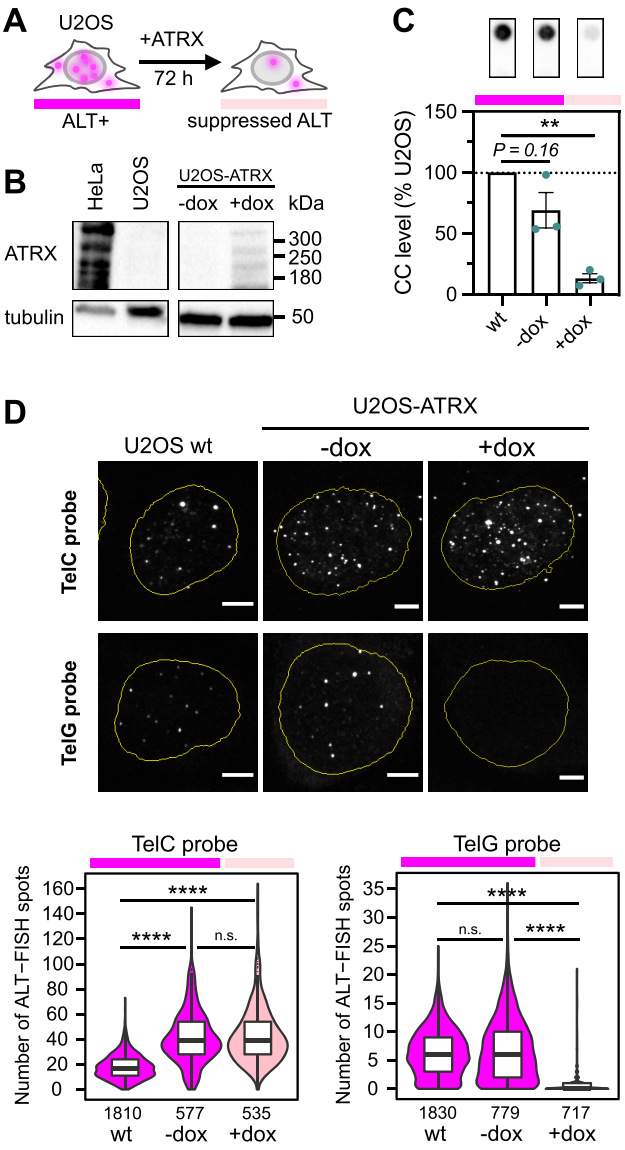

Figure 5. Detection of ATRX-mediated ALT suppression by ALT-FISH. (**A**) Scheme of ALT suppression by doxycycline (dox)-inducible ATRX re-expression in the ALT+ and ATRX-deficient U2OS cell line. (**B**) Western blot showing ATRX expression in transgenic U2OS-ATRX cells three days with/without dox. HeLa (ATRX wt) and U2OS wt are included as references. (**C**) Quantification of CC level changes upon ATRX re-expression with representative blots on top. Bar plot depicts mean and SEM of three independent induction experiments relative to U2OS wt. Values of $P = 0.16$ and $P = 0.0019$ (**) were calculated using a one-sample Student's *t*-test. (**D**) TelC and TelG ALT-FISH staining and nuclear spot number quantification for U2OS wt and U2OS-ATRX +/–dox. Count data were pooled from three independent induction experiments. Data from from Figure 1C for U2OS wt (four replicates) are included for comparison. Adjusted *P*-values from a pair-wise Wilcoxon rank sum test with BH correction were >0.05 (not significant, n.s.) or <2e–16 (****). The number of analyzed cells is given below. Boxplots depict the median with first and third quartile of the distribution. Scale bars are 5 μm.

fine a CC assay independent threshold for ALT positivity in a tissue region. The mean nuclear spot count of the combined controls was 0.1 spots/nucleus. The cutoff was defined as 1.5 times this value yielding a mean spot count per nucleus of 0.15. With this value the assay sensitivity and specificity were 0.91 and 0.89, respectively, with the CC signal as reference. The mean spot number per nucleus was also significantly different when comparing the ALT-positive to the ALT-negative cases within each entity (LMS: *P*-value = 0.047, NB: *P*-value = 0.002, unpaired Student's t-test) (Supplementary Figure S6E).

It is noted that the above type of ALT-FISH based ALT status assignment averages the signal across the imaged tissue region but ignores that typically also non-malignant cells are present, and that the ALT-FISH signal shows large differences between individual cells. To assess this heterogeneity of ALT activity for individual tumor sections, we developed a visualization approach, which maps back predefined groups of ALT activity onto the spatial tissue context to generate color-coded ALT activity maps. An example is shown for a tissue section from an ALT-positive LMS tumor (Figure 6A–C). Cell nuclei in the tissue images were classified into four ALT activity groups (ALT-negative, 0 spots; Low-ALT, 1–2 spots; ALT, 3–20 spots; super-ALT, >20 spots). The classification of the first three groups was informed by the previously determined cutoff used to separate ALT+ from ALT- cells in cell mixtures (>2 ALT-FISH spots, see Figure 2). For simplicity and visualization, the super-ALT cells were defined as having >20 spots. It is noted that this cutoff yielded cell fractions between 0.1 and 0.4% for the LMS and neuroblastoma tumors. Accordingly, an alternative approach would be to set it based on the specific distributions found in a larger sample set of a given tumor entity. The ALT activity map highlighted regions of particularly low or high ALT activity (Figure 6C, regions I-III). Similar to what was observed for cell lines (see Figure 3C), a nearest neighbor analysis (45) of this map for LMS L1.1 (L1.1 and L1.2 designates two different tissue sections from the same L1 tumor sample) suggested some preferential clustering of cells belonging to the same ALT activity group (Figure 6C).

ALT activity maps of multiple tumor tissue sections across both entities revealed substantial intra- and inter-tumor heterogeneity. This was particularly pronounced for the LMS samples, which displayed highly variable map profiles for the ALT-positive cases (Figure 6D). The normal tissue sample matched to the ALT-positive LMS tumor L3 showed very little ALT-FISH signal (<5% of nuclei with > 1 spot) and was comparable to the ALT-negative tumors L6–L9 (see Figure 6D). Strikingly, the ALT-positive NB tumors analyzed in this study exhibited an overall higher ALT activity as compared to the LMS samples (Figure 7C, Supplementary Figure S6B, D). We also observed heterogeneity among NB tumors that were classified as ALT-negative based on the CC assay. An exemplary case is shown for a section of the N5 tumor sample, which contains 14.8% of nuclei with 1–2 and 2.3% of nuclei with >2 ALT-FISH spots (Figure 7C, top row). This relatively small fraction of (lowly) ALT-positive cells indicates that this tumor sample is partly ALT-positive based on the ALT-FISH signal although it was classified as ALT-negative in the CC assay. To validate that a positive ALT-FISH signal is highly specific for tumor cells, we combined ALT-FISH and immuno-staining for the well-established neuroblastoma tumor marker NCAM (46,47) on one ALT-positive NB tumor section (Figure 7A). The tumor marker

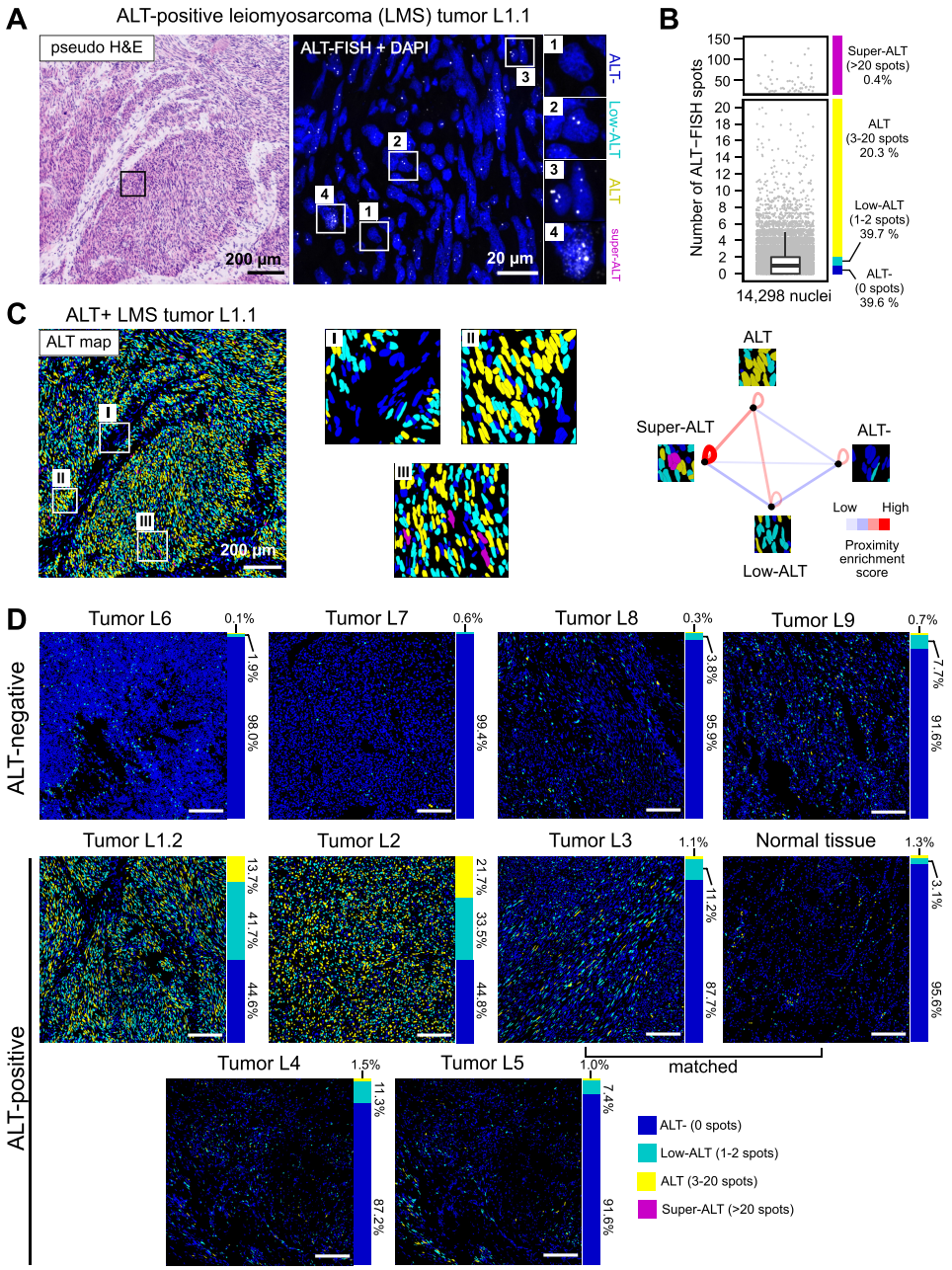

Figure 6. ALT-FISH analysis of leiomyosarcoma (LMS) tumor tissue. ALT status assignment is according to the CC analysis (Supplementary Figure S6A). See Supplementary Figure S6 and Supplementary Data Set 1 for additional information and ALT-FISH spot statistics of all LMS tumors. All scale bars are 200 μm. (**A**) Tissue section from an ALT-positive LMS tumor stained by pseudo H&E and TelC ALT-FISH. An overview image (∼1.3 mm x 1.3 mm) is shown in the H&E representation. The zoom-in (20 μm scale bar) shows the merged DAPI and ALT-FISH signals within a selected region. (**B**) Spot count distribution of the tumor section from panel A. Boxplot with jittered dots depicts the median with first and third quartile of the distribution. Note that the y-axis is interrupted for visualization of cells with >20 spots ($n = 52$) in the upper box. A total of 14 298 nuclei were segmented and binned into four ALT activity groups based on their spot counts (ALT-, Low-ALT, ALT, Super-ALT). Representative examples of nuclei with corresponding spot counts are highlighted in panel A. (**C**) Left: ALT activity map that projects color-coded ALT activity groups from panel B onto the entire imaged tissue region. Zoom-ins I-III illustrate the heterogeneity of ALT-FISH signals in different subregions. Right: Nearest neighbor analysis of the four ALT activity groups for LMS tumor L1.1. It suggests a preferential clustering of cells belonging to the same ALT activity group. (**D**) ALT activity maps of four ALT-negative, five ALT-positive LMS tumor tissue sections (L1–L9) and one matched normal tissue sample matched to tumor L3. The fraction of nuclei falling into each ALT activity group is visualized by stacked bar graphs next to the images. Samples L1.1 and L1.2 correspond to two different tissue sections from the same LMS tumor L1.

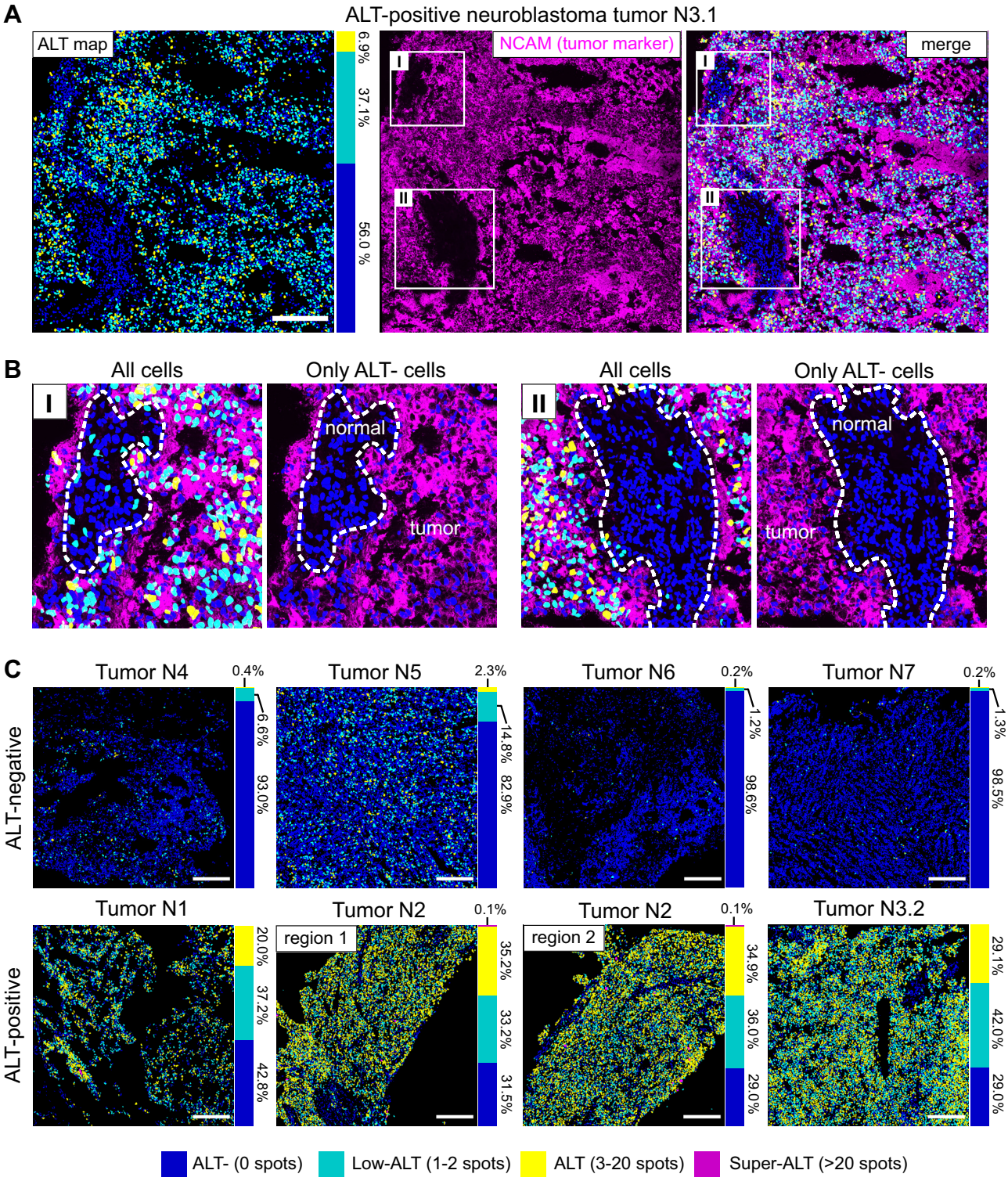

Figure 7. ALT-FISH analysis and tumor marker co-staining of neuroblastoma (NB) tumor tissue. ALT status assignment is according to the CC analysis (Supplementary Figure S6C). See Supplementary Figure S6 and Supplementary Data Set 1 for additional information and spot statistics of all NB tumors. All scale bars are 200 μm. (**A**) ALT activity map of an ALT-positive NB tumor tissue section stained by TelC ALT-FISH and immuno-staining against the neuroblastoma-specific tumor cell marker NCAM (magenta). (**B**) Distinct regions of low to no ALT activity (I, II) were overlaid with the regions that lacked NCAM signal, identifying them as non-tumor/normal tissue. Nuclei classified as ALT-negative (blue) were also present in NCAM-positive tissue regions, indicating heterogeneity within the tumor cell population. (**C**) ALT activity maps of four ALT-negative and three ALT-positive NB sections. Two adjacent regions (~1 mm^2 each) from the same section of ALT-positive tumor N2 are depicted. The fraction of nuclei falling into each ALT activity group is visualized by stacked bar graphs next to the images. Tumor N3.2 corresponds to an additional section of the tumor N3 sample analyzed in panel A (N3.1). Note that tumor N5 classified as ALT-negative in the CC assay displays a comparably high proportion of low-ALT cells based on the ALT map analysis.

was highly correlated with the ALT-FISH signal. NCAM-negative (non-tumor) regions of this tissue sample almost exclusively contained cell nuclei classified as ALT-negative. In contrast, NCAM-positive regions contained cell nuclei from all ALT activity groups. Thus, ALT-FISH can resolve the heterogeneity within tumor cell populations and distinguish between tumor cells and normal tissue. Furthermore, including an additional marker to distinguish regions of tumor and non-malignant cells on the tissue section could also be exploited to increase the specificity and sensitivity of ALT-FISH signal to classify tumors as ALT-positive or ALT-negative. Overall, our ALT-FISH results on tissue were in excellent agreement with the CC levels determined for the individual tumors across both entities and found a positive relationship between high ALT activity measured by ALT-FISH, high CC levels and mutated ATRX (Supplementary Figure S6A, C).

DISCUSSION

The ALT-FISH assay introduced here quantifies single-stranded DNA and RNAs containing the C- or G-rich telomere repeat sequences with single cell resolution *in situ*. Our method is universally applicable to adherent cell lines, cell suspensions and primary tumor tissue samples. ALT-FISH does not require proprietary chemistry or specialized reagents and can thus be implemented in a straightforward manner. In contrast to APB staining as an ALT marker, ALT-FISH exhibits a higher dynamic range and only requires a single isothermal hybridization reaction instead of antibody co-staining and co-localization image analysis. The ALT-FISH image data analysis is highly scalable as demonstrated here by analyzing ∼45 000 (cell lines) and >194 000 individual cell nuclei (tissue samples). Thus, it is well suited for high-throughput applications on different types of samples. Increased and heterogeneous telomere length as determined by denaturing telomere FISH has also been reported as quantifiable marker of ALT activity (48). However, accurate telomere length measurements are challenging to perform *in situ* and often yield only small differences.

In addition to high-throughput applications, ALT-FISH can be applied to investigate the dynamics, localization and interaction partners of single-stranded telomeric DNA/RNA species linked to the ALT mechanism, e.g. by combining it with immuno-staining. A staining with either the TelC or TelG probe was sufficient to determine the ALT status in the samples studied here. The TelC probe yielded a higher number of spots per cell with median numbers between 7–17 (TelC) or 3–6 (TelG) spots in ALT+ cell lines. A more comprehensive assessment of the different DNA/RNA species (e.g., TERRA abundance in combination with the C- and G-rich ssDNA repeats) is provided by the combined use of the TelC and TelG probes together with RNase treatment. Since TERRA can be up-regulated under a variety of conditions like specific mutations (42), viral infection (43) or tumorigenesis alone (44) it is, on its own, not a reliable ALT marker. In fact, RNase treatment revealed TERRA level decoupling from ALT activity in our ATRX induction model.

The precise quantitative relationship between recombination-based telomere elongation and the abundance of (partially) single-stranded species like CCs remains to be determined. However, we find that their levels can differ dramatically between individual cells. This heterogeneity was observed in a panel of cancer cell lines, three different ALT perturbation models and primary tumor tissue from two cancer entities, possibly representing differential telomere processing and/or stochastic inheritance or maintenance of these intermediates. A small cell population termed super-ALT cells here with particularly high ALT-FISH signal was consistently present in the ALT-positive cell lines and tissue sections. The occurrence of these cells is reminiscent of the 'ultrabright foci' phenomenon previously seen by denaturing telomere FISH (49). Our findings from weakly ALT+ and ALT-prone TERT+ cell lines suggest that the propensity to develop ALT is unequally distributed within a cell population. In line with ALT induction being a rare event, perturbations like ASF1 depletion may just shift the ALT-proneness of the entire population, resulting in a mixed population containing only a small fraction of outliers that activate ALT. These changes affecting only few cells are likely to be missed by bulk readouts like the CC assay.

The application of ALT-FISH to tumor tissue provides a new approach to resolve intra- and inter-tumor heterogeneity in cancer entities with high ALT prevalence as for example pediatric glioblastoma, neuroblastoma, leiomyosarcoma and pancreatic neuroendocrine tumors (23,24,50). The usefulness of native telomere FISH against C-rich repeats for assessing the ALT status was very recently also shown for mouse xenograft models and FFPE material from other tumor entities (51). Our results from leiomyosarcoma and neuroblastoma demonstrate the use of ALT-FISH for resolving TMM heterogeneity in a spatial context with high sensitivity. We identified a CC negative neuroblastoma tumor (tumor N5, Figure 7C) with a comparably high fraction of low ALT activity cells (∼15%). Such phenotypes could hint at TMM emergence or transitions within the tumor. As opposed to TERT+ tumors, ALT-positive neuroblastomas are slowly growing, but have a similar dismal outcome in children, while tumors without a TMM usually have a good prognosis (12). Thus, the ALT activity maps presented here may qualify as a tool for the detection of TMM emergence or transitions between different TMMs (ALT+, TERT+) in evolving neuroblastomas. Conducting these types of analyses on a larger cohort of patients could aid in explaining some of the patient-to-patient variability with respect to ALT activity, treatment response or disease outcome. Since ALT-FISH is compatible with other staining and microscopy-based applications, it will also support the development of strategies to identify novel ALT markers and drug targets.

DATA AVAILABILITY

Scripts and associated functions for the image analysis are available at https://github.com/RippeLab/ALT-FISH together with a detailed description for their application.

SUPPLEMENTARY DATA

Supplementary Data are available at NAR Online.

ACKNOWLEDGEMENTS

We thank Philipp Mallm, Armin Hadzic, Manuel Gunkel and Holger Erfle for help and discussions. The technical support by the DKFZ/NCT Sample Processing Laboratory and the DKFZ light microscopy facility as well as patient sample provision via the NCT Molecular Precision Oncology Program are gratefully acknowledged.
Author contributions: Study design: L.F., K.R. Acquisition of data: L.F., A.R., C.K., N.M., S.S. Analysis of data: L.F., A.R., N.M., S.M.T., E.K. Providing samples: S.A.S., F.W., S.F., P.C. Writing of manuscript: L.F., K.R. Manuscript reviewing: all authors. Supervision and coordination: K.R.

FUNDING

DFG [RI1283/16-1]; Baden-Württemberg Stiftung [METID41-STARFISH]; START-HD Explorer project of the University of Heidelberg; data storage service was supported by the Ministry of Science, Research and the Arts Baden-Württemberg; DFG [INST 35/1314-1 and 35/1503-1 FUGG]. Funding for open access charge: German Cancer Research Center provided to Karsten Rippe.
Conflict of interest statement. None declared.

REFERENCES

1. Harley,C.B., Futcher,A.B. and Greider,C.W. (1990) Telomeres shorten during ageing of human fibroblasts. *Nature*, **345**, 458–460.
2. Bryan,T.M., Englezou,A., Gupta,J., Bacchetti,S. and Reddel,R.R. (1995) Telomere elongation in immortal human cells without detectable telomerase activity. *EMBO J.*, **14**, 4240–4248.
3. Jiang,W.Q., Zhong,Z.H., Henson,J.D., Neumann,A.A., Chang,A.C. and Reddel,R.R. (2005) Suppression of alternative lengthening of telomeres by Sp100-mediated sequestration of the MRE11/RAD50/NBS1 complex. *Mol. Cell Biol.*, **25**, 2708–2721.
4. Zhang,J.M., Yadav,T., Ouyang,J., Lan,L. and Zou,L. (2019) Alternative lengthening of telomeres through two distinct break-induced replication pathways. *Cell Rep.*, **26**, 955–968.
5. Nabetani,A. and Ishikawa,F. (2009) Unusual telomeric DNAs in human telomerase-negative immortalized cells. *Mol. Cell Biol.*, **29**, 703–713.
6. Cesare,A.J. and Griffith,J.D. (2004) Telomeric DNA in ALT cells is characterized by free telomeric circles and heterogeneous t-loops. *Mol. Cell Biol.*, **24**, 9948–9957.
7. Oganesian,L. and Karlseder,J. (2011) Mammalian 5′ C-rich telomeric overhangs are a mark of recombination-dependent telomere maintenance. *Mol. Cell*, **42**, 224–236.
8. Oganesian,L. and Karlseder,J. (2013) 5′ C-rich telomeric overhangs are an outcome of rapid telomere truncation events. *DNA Repair (Amst)*, **12**, 238–245.
9. Mazzucco,G., Huda,A., Galli,M., Piccini,D., Giannattasio,M., Pessina,F. and Doksani,Y. (2020) Telomere damage induces internal loops that generate telomeric circles. *Nat. Commun.*, **11**, 5297.
10. Sampl,S., Pramhas,S., Stern,C., Preusser,M., Marosi,C. and Holzmann,K. (2012) Expression of telomeres in astrocytoma WHO grade 2 to 4: TERRA level correlates with telomere length, telomerase activity, and advanced clinical grade. *Transl. Oncol.*, **5**, 56–65.
11. Ng,L.J., Cropley,J.E., Pickett,H.A., Reddel,R.R. and Suter,C.M. (2009) Telomerase activity is associated with an increase in DNA methylation at the proximal subtelomere and a reduction in telomeric transcription. *Nucleic Acids Res.*, **37**, 1152–1159.
12. Hartlieb,S.A., Sieverling,L., Nadler-Holly,M., Ziehm,M., Toprak,U.H., Herrmann,C., Ishaque,N., Okonechnikov,K., Gartlgruber,M., Park,Y.G. *et al.* (2021) Alternative lengthening of telomeres in childhood neuroblastoma from genome to proteome. *Nat. Commun.*, **12**, 1269.
13. Fasching,C.L., Neumann,A.A., Muntoni,A., Yeager,T.R. and Reddel,R.R. (2007) DNA damage induces alternative lengthening of telomeres (ALT) associated promyelocytic leukemia bodies that preferentially associate with linear telomeric DNA. *Cancer Res.*, **67**, 7072–7077.
14. Grudic,A., Jul-Larsen,A., Haring,S.J., Wold,M.S., Lonning,P.E., Bjerkvig,R. and Boe,S.O. (2007) Replication protein a prevents accumulation of single-stranded telomeric DNA in cells that use alternative lengthening of telomeres. *Nucleic Acids Res.*, **35**, 7267–7278.
15. Yeager,T.R., Neumann,A.A., Englezou,A., Huschtscha,L.I., Noble,J.R. and Reddel,R.R. (1999) Telomerase-negative immortalized human cells contain a novel type of promyelocytic leukemia (PML) body. *Cancer Res.*, **59**, 4175–4179.
16. Chen,Y.A., Shen,Y.L., Hsia,H.Y., Tiang,Y.P., Sung,T.L. and Chen,L.Y. (2017) Extrachromosomal telomere repeat DNA is linked to ALT development via cGAS-STING DNA sensing pathway. *Nat. Struct. Mol. Biol.*, **24**, 1124–1131.
17. Ogino,H., Nakabayashi,K., Suzuki,M., Takahashi,E., Fujii,M., Suzuki,T. and Ayusawa,D. (1998) Release of telomeric DNA from chromosomes in immortal human cells lacking telomerase activity. *Biochem. Biophys. Res. Commun.*, **248**, 223–227.
18. Henson,J.D., Cao,Y., Huschtscha,L.I., Chang,A.C., Au,A.Y., Pickett,H.A. and Reddel,R.R. (2009) DNA C-circles are specific and quantifiable markers of alternative-lengthening-of-telomeres activity. *Nat. Biotechnol.*, **27**, 1181–1185.
19. Henson,J.D., Hannay,J.A., McCarthy,S.W., Royds,J.A., Yeager,T.R., Robinson,R.A., Wharton,S.B., Jellinek,D.A., Arbuckle,S.M., Yoo,J. *et al.* (2005) A robust assay for alternative lengthening of telomeres in tumors shows the significance of alternative lengthening of telomeres in sarcomas and astrocytomas. *Clin. Cancer Res.*, **11**, 217–225.
20. Osterwald,S., Worz,S., Reymann,J., Sieckmann,F., Rohr,K., Erfle,H. and Rippe,K. (2012) A three-dimensional colocalization RNA interference screening platform to elucidate the alternative lengthening of telomeres pathway. *Biotechnol. J.*, **7**, 103–116.
21. Osterwald,S., Deeg,K.I., Chung,I., Parisotto,D., Worz,S., Rohr,K., Erfle,H. and Rippe,K. (2015) PML induces compaction, TRF2 depletion and DNA damage signaling at telomeres and promotes their alternative lengthening. *J. Cell Sci.*, **128**, 1887–1900.
22. Gunkel,M., Chung,I., Worz,S., Deeg,K.I., Simon,R., Sauter,G., Jones,D.T.W., Korshunov,A., Rohr,K., Erfle,H. *et al.* (2017) Quantification of telomere features in tumor tissue sections by an automated 3D imaging-based workflow. *Methods*, **114**, 60–73.
23. Sieverling,L., Hong,C., Koser,S.D., Ginsbach,P., Kleinheinz,K., Hutter,B., Braun,D.M., Cortes-Ciriano,I., Xi,R., Kabbe,R. *et al.* (2020) Genomic footprints of activated telomere maintenance mechanisms in cancer. *Nat. Commun.*, **11**, 733.
24. Chudasama,P., Mughal,S.S., Sanders,M.A., Hubschmann,D., Chung,I., Deeg,K.I., Wong,S.H., Rabe,S., Hlevnjak,M., Zapatka,M. *et al.* (2018) Integrative genomic and transcriptomic analysis of leiomyosarcoma. *Nat. Commun.*, **9**, 144.
25. de Nonneville,A. and Reddel,R.R. (2021) Alternative lengthening of telomeres is not synonymous with mutations in ATRX/DAXX. *Nat. Commun.*, **12**, 1552.
26. Mender,I. and Shay,J.W. (2015) Telomerase Repeated Amplification Protocol (TRAP). *Bio. Protoc.*, **5**, e1657.
27. Deeg,K.I., Chung,I., Poos,A.M., Braun,D.M., Korshunov,A., Oswald,M., Kepper,N., Bender,S., Castel,D., Lichter,P. *et al.* (2017) Dissecting telomere maintenance mechanisms in pediatric glioblastoma. bioRxiv doi: https://doi.org/10.1101/129106, 20 April 2017, preprint: not peer reviewed.
28. O'Sullivan,R.J., Arnoult,N., Lackner,D.H., Oganesian,L., Haggblom,C., Corpet,A., Almouzni,G. and Karlseder,J. (2014) Rapid induction of alternative lengthening of telomeres by depletion of the histone chaperone ASF1. *Nat. Struct. Mol. Biol.*, **21**, 167–174.
29. Caudron-Herger,M., Pankert,T., Seiler,J., Nemeth,A., Voit,R., Grummt,I. and Rippe,K. (2015) Alu element-containing RNAs maintain nucleolar structure and function. *EMBO J.*, **34**, 2758–2774.
30. Toth,K.F., Knoch,T.A., Wachsmuth,M., Frank-Stohr,M., Stohr,M., Bacher,C.P., Muller,G. and Rippe,K. (2004) Trichostatin A-induced histone acetylation causes decondensation of interphase chromatin. *J. Cell Sci.*, **117**, 4277–4287.

31. Deeg,K.I., Chung,I., Bauer,C. and Rippe,K. (2016) Cancer cells with alternative lengthening of telomeres do not display a general hypersensitivity to ATR inhibition. *Front. Oncol.*, **6**, 186.
32. Elfer,K.N., Sholl,A.B., Wang,M., Tulman,D.B., Mandava,S.H., Lee,B.R. and Brown,J.Q. (2016) DRAQ5 and eosin ('D&E') as an analog to hematoxylin and eosin for rapid fluorescence histology of fresh tissues. *PLoS One*, **11**, e0165530.
33. Schindelin,J., Arganda-Carreras,I., Frise,E., Kaynig,V., Longair,M., Pietzsch,T., Preibisch,S., Rueden,C., Saalfeld,S., Schmid,B. *et al.* (2012) Fiji: an open-source platform for biological-image analysis. *Nat. Methods*, **9**, 676–682.
34. Pau,G., Fuchs,F., Sklyar,O., Boutros,M. and Huber,W. (2010) EBImage-an r package for image processing with applications to cellular phenotypes. *Bioinformatics*, **26**, 979–981.
35. Stringer,C., Wang,T., Michaelos,M. and Pachitariu,M. (2021) Cellpose: a generalist algorithm for cellular segmentation. *Nat. Methods*, **18**, 100–106.
36. Bahry,E., Breimann,L., Epstein,L., Kolyvanov,K., Harrington,K.I.S., Lionnet,T. and Preibisch,S. (2021) RS-FISH: precise, interactive and scalable smFISH spot detection using radial symmetry. bioRxiv doi: https://doi.org/10.1101/2021.03.09.434205, 09 March 2021, preprint: not peer reviewed.
37. Berthold,M.R., Cebron,N., Dill,F., Gabriel,T.R., Kötter,T., Meinl,T., Ohl,P., Sieb,C., Thiel,K. and Wiswedel,B. (2008) KNIME: the konstanz information miner. In: Preisach,C., Burkhardt,H., Schmidt-Thieme,L. and Decker,R. (eds). *Data Analysis, Machine Learning and Applications. Studies in Classification, Data Analysis, and Knowledge Organization*. Springer, Berlin, Heidelberg, pp. 319–326.
38. Stuart,T., Butler,A., Hoffman,P., Hafemeister,C., Papalexi,E., Mauck,W.M. 3rd, Hao,Y., Stoeckius,M., Smibert,P. *et al.* (2019) Comprehensive integration of single-cell data. *Cell*, **177**, 1888–1902.
39. Tokutake,Y., Matsumoto,T., Watanabe,T., Maeda,S., Tahara,H., Sakamoto,S., Niida,H., Sugimoto,M., Ide,T. and Furuichi,Y. (1998) Extra-chromosomal telomere repeat DNA in telomerase-negative immortalized cell lines. *Biochem. Biophys. Res. Commun.*, **247**, 765–772.
40. Komosa,M., Root,H. and Meyn,M.S. (2015) Visualization and quantitative analysis of extrachromosomal telomere-repeat DNA in individual human cells by Halo-FISH. *Nucleic Acids Res.*, **43**, 2152–2163.
41. Fasching,C.L., Neumann,A.A., Muntoni,A., Yeager,T.R. and Reddel,R.R. (2007) DNA damage induces alternative lengthening of telomeres (ALT)-associated promyelocytic leukemia bodies that preferentially associate with linear telomeric DNA. *Cancer Res.*, **67**, 7072–7077.
42. Yehezkel,S., Segev,Y., Viegas-Pequignot,E., Skorecki,K. and Selig,S. (2008) Hypomethylation of subtelomeric regions in ICF syndrome is associated with abnormally short telomeres and enhanced transcription from telomeric regions. *Hum. Mol. Genet.*, **17**, 2776–2789.
43. Deng,Z., Kim,E.T., Vladimirova,O., Dheekollu,J., Wang,Z., Newhart,A., Liu,D.M., Myers,J.L., Hensley,S.E., Moffat,J. *et al.* (2014) HSV-1 remodels host telomeres to facilitate viral replication. *Cell Rep.*, **9**, 2263–2278.
44. Deng,Z., Wang,Z., Xiang,C., Molczan,A., Baubet,V., Conejo-Garcia,J., Xu,X., Lieberman,P.M. and Dahmane,N. (2012) Formation of telomeric repeat-containing RNA (TERRA) foci in highly proliferating mouse cerebellar neuronal progenitors and medulloblastoma. *J. Cell Sci.*, **125**, 4383–4394.
45. Dries,R., Zhu,Q., Dong,R., Eng,C.L., Li,H., Liu,K., Fu,Y., Zhao,T., Sarkar,A., Bao,F. *et al.* (2021) Giotto: a toolbox for integrative analysis and visualization of spatial expression data. *Genome Biol.*, **22**, 78.
46. Phimister,E., Kiely,F., Kemshead,J.T. and Patel,K. (1991) Expression of neural cell adhesion molecule (NCAM) isoforms in neuroblastoma. *J. Clin. Pathol.*, **44**, 580–585.
47. Lipinski,M., Hirsch,M.R., Deagostini-Bazin,H., Yamada,O., Tursz,T. and Goridis,C. (1987) Characterization of neural cell adhesion molecules (NCAM) expressed by ewing and neuroblastoma cell lines. *Int. J. Cancer*, **40**, 81–86.
48. Henson,J.D., Neumann,A.A., Yeager,T.R. and Reddel,R.R. (2002) Alternative lengthening of telomeres in mammalian cells. *Oncogene*, **21**, 598–610.
49. Heaphy,C.M., de Wilde,R.F., Jiao,Y., Klein,A.P., Edil,B.H., Shi,C., Bettegowda,C., Rodriguez,F.J., Eberhart,C.G., Hebbar,S. *et al.* (2011) Altered telomeres in tumors with ATRX and DAXX mutations. *Science*, **333**, 425.
50. MacKenzie,D. Jr, Watters,A.K., To,J.T., Young,M.W., Muratori,J., Wilkoff,M.H., Abraham,R.G., Plummer,M.M. and Zhang,D. (2021) ALT positivity in human cancers: prevalence and clinical insights. *Cancers (Basel)*, **13**, 2384.
51. Claude,E., de Lhoneux,G., Pierreux,C.E., Marbaix,E., de Ville de Goyet,M., Boulanger,C., Van Damme,A., Brichard,B. and Decottignies,A. (2021) Detection of alternative lengthening of telomeres mechanism on tumor sections. *Mol. Biomed.*, **2**, 32.